Applied Catalysis B: Environmental 225 (2018) 364–378

Contents lists available at ScienceDirect

Applied Catalysis B: Environmental

journal homepage: www.elsevier.com/locate/apcatb

Streamlining of the synthesis process of Pt/carbon xerogel electrocatalysts with high Pt loading for the oxygen reduction reaction in proton exchange membrane fuel cells applications

Anthony Zubiaur*, Nathalie Job*

Department of Chemical Engineering – Nanomaterials, Catalysis, Electrochemistry, University of Liège (B6a), B-4000 Liège, Belgium

ARTICLE INFO

Keywords:
Platinum electrocatalyst
Carbon xerogel
Platinum particles synthesis
ORR
PEMFC

ABSTRACT

Pt/carbon xerogel catalysts were synthesized by different methods. The strong electrostatic adsorption (SEA) method, which consists in enhancing electrostatic interactions between the support and the precursor, was first modified in order to avoid any Pt loss (charge enhanced dry impregnation, CEDI). In a second step, the synthesis was rationalized to speed up the reduction (liquid phase reduction with sodium borohydride, $NaBH_4$). The synthesis procedure was further simplified in order to obtain one-step procedures, such as (i) reduction of highly loaded platinum solution by sodium borohydride, (ii) formic acid reduction, and (iii) colloid synthesis. All the catalysts were analyzed by physicochemical and electrochemical methods. They are compared to a reference commercial catalyst (Tanaka). The best performances are obtained by the SEA, the CEDI and the formic acid reduced catalysts, the performance of which are at least equal to, or even higher (up to 20–25% in mass activity) than those of the commercial reference. From these three methods, the only one-step method is the formic acid reduction, which allows avoiding time-consuming drying and H_2 reduction steps.

1. Introduction

Proton exchange membrane fuel cells (PEMFCs) are promising and eco-friendly power generators. However, they are not widely commercialized yet. This is especially because of the high cost of the device, which is partly due to one of its major component: the catalytic layer. Indeed, common catalytic layers are constituted of Pt or Pt-based nanoparticles supported on high surface area carbon (Pt/HSAC) [1]. These catalytic layers usually display high Pt loading, which increases the fuel cell price as Pt is an expensive metal with supply limitations [2,3]. One of the fuel cell researchers' main objectives is therefore to decrease the Pt loading of the catalytic layers while keeping high performances.

To do so, the increase of the Pt dispersion on the support was studied in order to increase the number of active sites available for reaction, *i.e.* the number of Pt atoms at the surface of the particles. The number of active sites increases when the Pt particle size decreases, *i.e.* when the Pt specific surface area increases. Indeed, the smaller the Pt particle size, the higher the Pt specific surface area. However, too small Pt nanoparticles lead to a decrease in activity of the surface Pt atoms for most of the reactions performed in PEMFCs, such as the oxygen reduction reaction (ORR). Indeed, these reactions are structure-sensitive [4]. So, the specific activity (*i.e.* current per surface unit of Pt) for the ORR increases with the particle size (up to several tens of nm). Therefore, the optimal Pt nanoparticles size, resulting in best mass activity (*i.e.* current per mass unit of Pt) is around 3–4 nm [5,6].

Over the years, many methods to synthesize Pt/carbon catalysts with high Pt loading and particle size distribution suitable for applications in PEMFCs have been developed [7,8]. Among the most popular ones, one can cite the impregnation of the support using a metal precursor (followed by drying and reduction treatment) and the impregnation-precipitation methods (where the metal precursor is directly reduced to precipitate onto the support), colloidal techniques (where a Pt particle colloid is first formed, then contacted with the support) [9], polyol methods (where a metal precursor is reduced by polyhydroxylic alcohol, often in the presence of a surfactant) [10,11], the deposition of metal clusters from the gas phase (by physical/chemical vapor deposition or by metal sputtering) [12,13] or even plasma-derived techniques (where the Pt precursor is contacted with the support and decomposed by plasma treatment) [14]. Regarding the support, many carbons have been used, from classical carbon blacks to nanostructures like nanotubes or graphene [15,16]. In the last decade, carbon xerogels (CXs), *i.e.* nanostructured carbons prepared by drying and pyrolysis of organic gels, have been used by a few research groups [17–24]. The

* Corresponding authors.
E-mail addresses: A.Zubiaur@ulg.ac.be (A. Zubiaur), Nathalie.Job@ulg.ac.be (N. Job).

https://doi.org/10.1016/j.apcatb.2017.11.059
Received 13 July 2017; Received in revised form 14 November 2017; Accepted 22 November 2017
Available online 24 November 2017
0926-3373/ © 2017 Elsevier B.V. All rights reserved.

main interest of such supports lies in their better electrode architecture control and enhanced mass transport properties [18]. Recently, in an effort to synthesize Pt/carbon xerogel catalysts with high metal loading and high dispersion, the strong electrostatic adsorption (SEA) method [25–27] was especially developed on such nanostructured carbon supports. The SEA technique consists in maximizing the electrostatic interactions between the metal precursor and the support by adjusting the pH of the carbon/water/Pt precursor slurry to the adequate value. This value depends on the surface chemistry of the support and on the nature of the Pt precursor. Due to the presence of various oxygenated surface groups, the carbon support protonates/deprotonates at low/high pH value. This enhances the adsorption of anions/cations, respectively. For example, in the case of the impregnation of CXs by hexachloroplatinic acid (CPA, H_2PtCl_6) aqueous solutions (1000 ppm_{Pt}), the highest Pt uptake occurs at a final pH around 2.5, which yields a Pt loading ca. 8–10 wt.% [27]. In order to achieve high Pt mass fraction without sacrificing the dispersion, the SEA procedure can be performed several times consecutively with fresh Pt precursor solution [27] or with the same (recycled) Pt precursor solution [22].

However, the size of the Pt particles synthesized by the SEA technique is *ca.* 2 nm [22], which is below the optimal value for PEMFC catalysts [5,6]. Another drawback of this method is the complexity of the procedure to obtain catalysts with high Pt loading. Indeed, in order to synthesize highly loaded Pt/CX catalysts (> 20 wt.%), the CX undergoes several synthesis steps, *i.e.* adsorption of Pt ions, filtration, drying, and reduction under hydrogen, which must be repeated several times since one single cycle leads to 8 wt.% in Pt. All these steps are time-consuming. As an example, three days at least are required to synthesize 20 wt.% Pt/CX *via* SEA (1 day for each impregnation-reduction cycle). This implies that some adaptations/modifications must be performed on the synthesis procedure in order to obtain easy-to-make Pt/CX catalysts with high performances.

The purpose of the first synthesis modification performed in our previous studies so far was to avoid Pt loss. To do so, the charge enhanced dry impregnation (CEDI) method was used [28]. It combines the advantages of (i) the SEA method, as the pH of the Pt precursor solution is fixed at an optimal value in order to maximize the interactions between the metallic ions and the support, which leads to a high metal dispersion, and (ii) the dry impregnation (DI) method, as the volume of the precursor solution strictly corresponds to that necessary to fill the pores of the support. This strategy avoids Pt loss during the synthesis. Cao et al. [28] synthesized Pt/CX catalysts with 10 wt.% Pt loading in one impregnation-reduction cycle with CPA as precursor.

Another modification of the synthesis was investigated in previous works: one-step deposition methods. These allow to deposit large Pt quantity on CX in one single impregnation-reduction step. One-step syntheses lead to highly loaded Pt/CX catalysts synthesized within a few hours, whatever the final loading.

One of these one-step syntheses, developed by Alegre et al. [29], uses sodium borohydride (SB) as a reductant. It consists in the impregnation of the CX support, followed by reduction with SB, in liquid phase. 20 wt.% Pt catalyst on CX were prepared by this technique [29].

Another one-step synthesis, also developed by Alegre et al. [29], uses formic acid (FA, HCOOH) as reductant, in liquid phase. The aim of the FA reduction is to control the reduction speed which is not possible with SB reduction. Indeed, SB-reduced catalysts usually display large Pt particle size distribution (PSD) due to the high reduction speed induced by SB [29,30]. In the above-mentioned study, Alegre et al. synthesized 20 wt.% Pt on CX catalyst *via* FA reduction.

Another one-step method, the synthesis of Pt/C catalysts using a Pt colloid, was developed by Pasqualeti et al. [31]. The method consists in the synthesis of a Pt colloid suspension followed by the addition of a carbon support onto which adsorption of the Pt particles occurs. The aim of the colloid synthesis is to control the Pt particle size while reducing Pt ions with SB, by using tri-sodium citrate (tSC, $Na_3C_6H_5O_7$) as a surfactant. Pasqualeti et al. synthesized 20 wt.% Pt on carbon black (Vulcan XC-72R) catalysts [31].

All these syntheses were reproduced for this work. Some of them were modified in order to change the loading: (i) the CEDI method was repeated up to four times to increase the Pt loading of the catalysts; (ii) the FA reduction synthesis and the colloid synthesis were modified in order to produce 10, 30, and 40 wt.% Pt/CX catalysts in addition to the 20 wt.% Pt/CX catalyst.

Finally, another method based on SEA was performed. Contrary to SEA and CEDI synthesis (the other two method based on SEA), in which reduction step was performed under gaseous hydrogen, this method uses SB reduction in liquid phase. The purpose of this liquid-phase reduction is to fasten the synthesis of highly loaded Pt/CX catalysts obtained by multiple impregnation-reduction methods. These SB-reduced catalysts were compared to SB-reduced catalysts synthesized *via* the one-step synthesis in order to study the differences between one-step deposition and multiple impregnation-reduction steps methods.

This work will focus on these syntheses with the aim of simplifying at best the synthesis process while optimizing the catalyst performances. Note that we decided to focus here on synthesis methods that can be conducted at room temperature and under air, which excludes the commonly used polyol technique [11,10], the latter requiring relatively high synthesis temperatures (393–473 K) and deaerated solutions.

2. Experimental

2.1. Reagents

The solid reagents used in this work were resorcinol $C_6H_6O_2$ (Merck, for synthesis), sodium carbonate Na_2CO_3 (Acros Organics, 99.5% extrapure, anhydrous), dihydrogen hexachloroplatinate (IV) hexahydrate $H_2PtCl_6{\cdot}6H_2O$ (Alfa Aesar, 99.9% metal basis, crystalline), sodium hydroxide NaOH (Acros Organics, extrapure, pellets), sodium borohydride $NaBH_4$ (Merck, fine granular for synthesis), and tri-sodium citrate dihydrate $Na_3C_6H_5O_7{\cdot}2H_2O$ (Merck, EMSURE® for analysis).

The liquid reagents used in this work were formaldehyde solution CH_2O (Sigma Aldrich, ACS reagent 37 wt.% in water, contains 10–15% methanol as stabilizer), hydrochloric acid HCl (Acros Organics, for analysis min. 35 wt.% solution in water), nitric acid HNO_3 (Merck, 65% for analysis), ultrapure water H_2O (18 MΩ cm), formic acid HCOOH, (Merck, 99% for synthesis), sulfuric acid H_2SO_4 (Merck, 96 wt.% Suprapur® for electrochemical measurements or Merck, 98% EMSURE®, for analysis for cleaning solution), hydrogen peroxide H_2O_2 (Merck, 30% Perhydrol®, EMSURE®, stabilized for higher storage temperature, for analysis), and Liquion™ solution (Ion Power, LQ-1105, 1100EW, 5 wt.%).

The gaseous reagents used in this work were nitrogen N_2 (Air Liquide, *α*1), hydrogen H_2 (Air Liquide, *α*1), carbon monoxide CO (Air Liquide, N47), argon Ar (Air Liquide, *α*1), and oxygen O_2 (Air Liquide, *α*1).

2.2. Syntheses

Carbon xerogel support. CX used in this work was prepared by drying and pyrolysis of a resorcinol-formaldehyde gel. This synthesis is described elsewhere [22]. Briefly, the gel was obtained by polycondensation of resorcinol with formaldehyde in water. The resorcinol/formaldehyde molar ratio, *R/F*, was set at 0.5, the resorcinol/sodium carbonate molar ratio, *R/C*, was chosen equal to 1000 and the dilution ratio, *D*, *i.e.* the solvent/(resorcinol and formaldehyde) molar ratio, was fixed at 5.7. These values led to a CX with a meso-macropore size distribution centered at 80 nm and a BET specific surface area of 567 $m^2\ g_{Pt}{}^{-1}$. After gelling and aging in an oven at 358 K, the obtained gel was dried under vacuum at 423 K, then ground with a planetary mill (PULVERISETTE 6, classical line, Fritsch) at 400 rpm during 70 min in order to obtain particles with a diameter of a few micrometers

according to a procedure developed in another work [32]. After grinding, the gel was pyrolyzed at 1073 K under nitrogen flow. The resulting CX particles exhibit a mean size of 7 μm.

Strong electrostatic adsorption (SEA). The SEA method [26] was already studied and applied on CX [27,22]. The synthesis procedure is as follows [22]: (i) the pH of 0.567 L of 1.75 $g_{Pt}\,L^{-1}$ hexachloroplatinic acid (CPA, $H_2PtCl_6{\cdot}6H_2O$) aqueous solution (8.97 mmol L^{-1}) was adjusted to 2.5, *i.e.* to the optimal pH value leading to maximum Pt uptake [27], with 0.5 mol L^{-1} HCl and NaOH solutions; (ii) 1 g of CX was added to the solution, *i.e.* the amount of CX corresponding to a surface loading of 1000 $m^2\,L^{-1}$; (iii) the suspension was stirred for 1 h; (iv) filtered; (v) dried at 393 K in an oven under air overnight; (vi) reduced under 0.04 mmol s^{-1} H_2 flow at 473 K for 1 h. In order to synthesize several catalysts with various Pt loadings, the Pt deposition was repeated from one to five times on the same support with the same impregnation solution, the pH of which is readjusted to the optimal value at each impregnation [22]. After the last impregnation, each catalyst underwent its last reduction step at 723 K during 5 h in order to remove the chlorine bound to the Pt particles. Indeed, high reduction temperature is necessary to completely clean the Pt particle surface from residual chlorine [33].

Charge enhanced dry impregnation (CEDI). The CEDI procedure is the following [28]: (i) 0.23 g of CPA were dissolved in 3 mL of deionized water; (ii) the initial pH was fixed at 1.8 with HNO_3; (iii) the precursor solution was added to 1 g of CX by 50 μL steps; (iv) the obtained paste was softly, manually stirred to homogenize it at best; (v) the mixture was dried at room temperature during 48 h; (vi) the sample was reduced under 0.04 mmol s^{-1} H_2 flow at 523 K for 1 h. As the CEDI method yields 10 wt.% Pt/CX, this procedure was repeated from one to four times in order to increase the amount of Pt deposited on the support. After their last impregnation, half of each catalyst was reduced as before (523 K for 1 h) but the other half underwent the last reduction step at 723 K during 5 h in order to study the effect of the temperature reduction on the CEDI synthesis.

Sodium borohydride reduction (SB). The SB synthesis proceeds as follows: (i) 1 g of CX was mixed in 200 mL of CPA solution with high concentration (4.8 $g_{Pt}\,L^{-1}$); (ii) the pH of the suspension was fixed at 2.5 with 0.5 mol L^{-1} NaOH solution; (iii) the suspension was stirred during 30 min; (iv) filtered; (v) the impregnated support was then suspended in ultrapure water with pH fixed at the optimal value for impregnation with CPA, *i.e.* 2.5; (vi) 0.25 g of sodium borohydride (SB) was added to the suspension in order to reduce the Pt ions into metallic Pt; (vii) after 5 min, the suspension was filtered; (viii) the catalyst was rinsed 5 times by 125 mL of ultrapure water, then (ix) dried in an oven under air at 333 K overnight. In order to reach higher Pt loading, the deposition was repeated up to eight times by recycling the CPA solution. In this work, only the catalysts which underwent 2, 4, 6, and 8 Pt depositions were studied. Note that, after reduction, the filtrate was analyzed by ICP-AES to check for Pt presence due to desorption of unreacted Pt precursor from carbon during the reduction procedure. Measured concentrations were in all cases lower than 1 ppm, which seems to indicate that the Pt reduction was fully achieved. However, this does not guarantee that all Cl is removed from the Pt surface. To check for this problem, half of each catalyst was characterized without any post-treatment while the other half underwent another reduction step under 0.04 mmol s^{-1} H_2 flow at 723 K for 5 h in order to clean the particles surface [33] and to compare with previous catalysts.

SB reduction synthesis was also performed *via* a one-step method in order to further fasten the synthesis procedure by removing the multiple impregnation-reduction steps. The one-step SB reduction procedure to synthesize 20 wt.% Pt catalyst is as follows: (i) 0.3 g of CX were dispersed in 200 mL of ultrapure water; (ii) 130 mL of 3 mmol L^{-1} CPA solution was added to the suspension; (iii) the pH of the mixture was fixed at 5.0 with 0.5 mol L^{-1} NaOH solution; (iv) 130 mL of 25 mmol L^{-1} SB solution was slowly added in order to reduce the Pt precursor into metallic Pt; (v) after 1 h stirring, the suspension was filtered; (vi) the catalyst was rinsed 5 times with 125 mL of ultrapure water; (vii) dried at 333 K in an oven under air overnight. This procedure differs from that of Alegre et al. [29] in the following 5 points: (i) as they were not explicitly mentioned, the mass and volume of reagents were chosen equal to 0.3 g of CX, 200 mL of ultrapure water, 130 mL of 3 mmol L^{-1} CPA aqueous solution, and 130 mL of 25 mmol L^{-1} SB aqueous solution; (ii) the addition of CPA into the suspension was not preformed under sonication; (iii) the temperature was not maintained at 291 K but performed at room temperature; (iv) a stirring step of 1 h was performed after the addition of SB, and (v) the washing step after the filtration, not detailed in [29], was performed as explained above. The differences are mainly due to the lack of information in the original article and to the simplification of the method.

Formic acid reduction. The FA method allows to synthesize Pt/CX catalysts of various Pt loading in one single Pt deposition step. For the 20 wt.% Pt/CX, the synthesis procedure is as follows: (i) 0.3 g of CX were dispersed in 200 mL of 2 mol L^{-1} FA solution; (ii) the suspension was heated to 353 K in an oil bath; (iii) 100 mL of 4 mmol L^{-1} CPA solution was added by 10 mL steps; (iv) after 1 h stirring, the suspension was filtered; (v) the catalyst was then washed 5 times with 125 mL of ultrapure water, then (vi) dried at 333 K in an oven under air overnight. The differences between the procedure from Alegre et al. [29] and the procedure just described are the following: (i) as they were not explicitly mentioned, the mass and volume of reagents were chosen equal to 0.3 g of CX, 200 mL of 2 mol L^{-1} FA solution, 100 mL of 4 mmol L^{-1} CPA aqueous solution, and stepwise addition of 10 mL volumes; (ii) a stirring step of 1 h was added after the addition of the CPA solution, and (iii) the washing step after the filtration, not detailed in [29], was performed as explained above. Again, the differences are mainly due to the lack of information in the original article, which does not describe all steps in details.

Colloid synthesis. The Pt colloid method allows to synthesize Pt/CX catalyst of various Pt loading in one single Pt deposition step. For the 20 wt.% Pt/CX, the synthesis procedure is as follows: (i) 50 mL of 14 mmol L^{-1} tri-sodium citrate (tSC) were added to 1.6 L of 0.2 mmol L^{-1} CPA solution; (ii) after 5 min stirring, 60 mL of ultrapure water containing 60 mg of SB and 200 mg of tSC were added to the solution; (iii) 90 min after the SB addition, 0.25 g of CX were added to the colloid suspension; (iv) after 48 h stirring, the suspension was filtered; (v) the catalyst was then rinsed 5 times with 150 mL of ultrapure water, then (vi) dried in an oven under air at 333 K overnight. This synthesis procedure differs from that of Pasqualeti et al. [31] in the following 6 points: (i) since the quantity of CPA was not mentioned in [31], it was chosen equal to 0.32 mmol; (ii) contrary to the procedure in the [31], tSC was added after CPA; (iii) waiting steps after tSC addition (5 min) and SB addition (90 min) were added; (iv) the quantity of carbon to add was not mentioned, so it was chosen equal to 0.25 g: (v) the carbon suspension was not sonicated; (vi) the drying step was performed as described above instead of kiln-drying at 343 K for 24 h. These differences are mainly due to the replacement of carbon black (Vulcan XC-72R) by CX, to the missing information in the article, and to some simplifications of the method.

List of samples. The samples are named following their synthesis method – SEA (strong electrostatic adsorption), CEDI (charge enhanced dry impregnation), SB (sodium borohydride reduction), FA (formic acid reduction), Col (tri-sodium citrate Pt colloid) – followed by, in the case of multiple impregnations method (SEA, CEDI, and SB), the number of impregnation steps they underwent after a slash (/) or, in the case of single deposition step method (SB, FA, and Col), the targeted Pt weight percentage after a hyphen (-). If the catalyst was reduced under H_2 flow at 723 K during 5 h after the synthesis, the suffix 723 is added after the method name. For example, SB/6 is the Pt/CX catalyst reduced by SB which underwent six impregnation-reduction cycles, SB723/6 is the sample reduced by SB which underwent six impregnation-reduction cycles and, after the synthesis, was reduced at 723 K under H_2 flow for 5 h. SB-20 is the sample reduced by SB which target Pt loading is equal

Table 1
List of samples synthesized *via* multiple impregnation methods.

Catalyst	Synthesis method	n_{impr}	$T_{red,f}$ (K)	$t_{red,f}$ (h)
SEA/1	SEA	1	723	5
SEA/2	SEA	2	723	5
SEA/3	SEA	3	723	5
SEA/4	SEA	4	723	5
SEA/5	SEA	5	723	5
CEDI/1	CEDI	1	523	1
CEDI/2	CEDI	2	523	1
CEDI/3	CEDI	3	523	1
CEDI/4	CEDI	4	523	1
CEDI723/1	CEDI	1	723	5
CEDI723/2	CEDI	2	723	5
CEDI723/3	CEDI	3	723	5
CEDI723/4	CEDI	4	723	5
SB/2	SB reduction	2	–[a]	–[a]
SB/4	SB reduction	4	–[a]	–[a]
SB/6	SB reduction	6	–[a]	–[a]
SB/8	SB reduction	8	–[a]	–[a]
SB723/2	SB reduction	2	723	5
SB723/4	SB reduction	4	723	5
SB723/6	SB reduction	6	723	5
SB723/8	SB reduction	8	723	5

n_{impr}: number of impregnation-reduction cycles underwent by the catalyst; $T_{red,f}$: temperature of the final reduction step under H_2; $t_{red,f}$: duration of the final reduction step under H_2.
[a] Not reduced under H_2.

Table 2
List of samples synthesized *via* one-step deposition methods.

Catalyst	Synthesis method	Pt_{target} (wt.%)
SB-20	SB reduction	20
FA-10	FA reduction	10
FA-20	FA reduction	20
FA-30	FA reduction	30
FA-40	FA reduction	40
Col-10	tSC Pt colloid	10
Col-20	tSC Pt colloid	20
Col-30	tSC Pt colloid	30
Col-40	tSC Pt colloid	40

Pt_{target}: Pt loading targeted by the one-step deposition synthesis.

to 20 wt.% (single impregnation). All the sample labels are listed in Table 1 for catalysts synthesized *via* multiple impregnation methods (SEA, CEDI, and SB) and in Table 2 for catalysts synthesized *via* one-step deposition methods (SB, FA, and Col). One commercial catalyst (Pt/HSAC Tanaka 37 wt.%, provided by Paxitech) is used as reference and labeled Ref.

2.3. Physicochemical characterization

The metal weight percentages of the catalysts were measured by Inductively Coupled Plasma–Atomic Emission Spectroscopy (ICP-AES) using an ICAP 6500 THERMO device. The solutions for the analyses were prepared as follows: an aliquot of the catalyst sample (30 or 50 mg, depending on the assumed Pt loading) was weighed and burned in air at 823 K for 24 h. The remaining ashes were digested in 8 mL aqua regia at 393 K, and the solution was transferred in a 100 mL calibrated flask which was finally filled by deionized water. Each sample was analyzed twice for measurement reproducibility (less than 3% difference was observed).

The particles were observed by Transmission Electron Microscopy (TEM) with a Jeol 2010 transmission electron microscope (200 kV, LaB_6 filament). An aliquot of the catalyst sample was suspended in 20 mL of ethanol. After 15 min of sonication in an ultrasonic bath, a drop of the suspension was deposited on a polymer-covered copper grid.

Image analysis was applied to the TEM micrographs (on 200 particles at least) in order to calculate the average diameter of particles, d_{TEM}, the standard deviation, σ, the surface-weighed average diameter of particles, d_s, and the volume-weighed average diameter of particles, d_v:

$$d_s = \frac{\Sigma n_i d_i^3}{\Sigma n_i d_i^2} \quad (1)$$

$$d_v = \frac{\Sigma n_i d_i^4}{\Sigma n_i d_i^3} \quad (2)$$

where n_i is the number of particles with diameter d_i [34]. d_s and d_v can be compared to the CO equivalent particle diameter obtained from CO stripping, d_{CO}, and to the average crystallite size obtained from X-ray diffraction (XRD), d_{XRD}, respectively (see below). Indeed, CO stripping (see Section 2.4) is a surface-sensitive technique, as it is a surface measurement method, while XRD is a volume-sensitive technique as large crystallites impact more XRD diffractograms.

The catalysts powders were analyzed by X-Ray Diffraction with a Siemens D5000 goniometer using the $Cu_{K\alpha}$ line (Ni filter). After baseline (C signal) subtraction, average crystallite sizes, d_{XRD}, were calculated from the diffraction peak width by Scherrer's equation [34]:

$$d_{XRD} = \frac{k\lambda}{\beta \cos\theta} \quad (3)$$

where k is a dimensionless shape factor and equals 0.89 in the case of spherical Pt nanoparticles, λ is the X-ray wavelength ($Cu_{K\alpha}$: 1.5456 nm), β is the full width at half the maximum intensity (FWHM), and θ is the Bragg angle. Obviously, the smaller and broader the diffraction peaks, the more imprecise the measurements of FHWM and the calculations of d_{XRD}. As XRD is a volume-sensitive analysis, d_{XRD} corresponds to an average volume diameter of particles (if they are monocrystalline) and can be compared to d_v [34].

2.4. Electrochemical characterization

Material. All the glassware was cleaned by immersion in a H_2SO_4:H_2O_2 solution overnight and thoroughly rinsed with ultrapure water (Millipore, 18 MΩ cm). The electrolytic solutions were prepared from ultrapure water and H_2SO_4 (98% Suprapur®, Merck).

Catalytic layer preparation. To measure the electrochemical properties of the catalysts, inks were first prepared. The ink composition was chosen to keep the amount of carbon constant, regardless of the metal loading [35]. For each sample, the amount of catalyst containing 19.8 mg of CX was crushed in a mortar then mixed with 755 mg of ultrapure water and 466 mg of 5 wt.% Nafion® solution. In order to blend it homogeneously, the mixture was then processed in an ultrasonic bath for 15 min. Once the ink was homogeneous, 10 µL of ink were deposited on a glassy carbon (GC) disk (5 mm in diameter) and sintered at 343 K during 20 min to evaporate the solvents and stick the catalyst onto the GC disk. The catalytic layer deposited on the GC disk composes the working electrode for all electrochemical measurements. In the case of CX-supported catalysts, this procedure yields active layers of identical thickness onto the GC disk (*i.e.* resulting in identical mass-transport limitation within the layer [35]). All the obtained coatings were visually homogeneous, without obvious cracks or wrinkles, even though the catalytic layers based on carbon xerogel supports were rougher than those obtained with the carbon-black-supported reference catalyst.

Electrolyte and wetting procedure. During all measurements, the working electrode was immersed in an electrolyte constituted of 1 M H_2SO_4 aqueous solution. H_2SO_4 solution was used in order to keep close to the real PEMFC environment. The use of liquid electrolyte should

ensure full wetting of the metal particles. Note that measurements in $HClO_4$ were also performed: even though absolute activity differences were observed, the trends between the various samples did not change significantly. In order to ensure that all the pores, *i.e.* both the extragranular and the mesoporous intergranular porosities, were fully filled, a drop of electrolyte was deposited onto the catalytic layer. Then, the electrode was put under vacuum in order to outgas the layer by bubbling air through the drop. Once no air bubbles were visible, the electrode and the drop were put back under atmospheric pressure so that the electrolyte filled the empty porosity of the layer. This wetting procedure ensures that the catalyst wetting is complete and that the Pt utilization factor is close to 100%. Indeed, previous works [27,22] performed on similar systems showed good consistency between the Pt specific surface area measured after using this wetting procedure and the surface calculated from TEM micrographs. Finally, the electrochemical measurements were usually steady, which also hints at good wetting of the layer.

Pretreatment of catalysts. Prior to any measurement, the electrolyte was deaerated by Ar bubbling. Then, sixteen voltammetry cycles were performed between 0.05 V *vs.* NHE and 1.23 V *vs.* NHE at a scanning speed of 0.05 V s^{-1}. Moreover, after each measurement, three voltammetry cycles with the same scanning speed and potential boundaries were recorded in order to monitor the three-electrode setup and check for any disturbance of the catalyst state (*e.g.* loss of powder on the GC electrode).

CO stripping voltammetry. The Pt specific surface area was measured by CO stripping voltammetry [36–38]. The procedure was initiated by the application of a steady potential of 0.1 V *vs.* NHE to the working electrode, while gaseous CO was bubbled in the electrolyte solution for 6 min. After an Ar purge of 39 min in order to remove the CO dissolved in the electrolyte (still at 0.1 V *vs.* NHE), the CO chemisorbed at the surface of the particles was electrooxidized into CO_2 by increasing the electrode potential from 0.05 to 1.23 V *vs.* NHE at 20 mV s^{-1}. The potential was then cycled between 0.05 and 1.23 V *vs.* NHE at the same scan speed for two more cycles. This results in three recorded cycles, *i.e.* the first cycle in which the peaks from the CO electrooxidation occur and two other cycles which are cyclic voltammetry cycles performed at 20 mV s^{-1}, as all the adsorbed CO was electrooxidized during the first cycle. As the third cycle represents the background of the CO stripping measurement, it is subtracted from the first in order to isolate the CO electrooxidation peak. The Pt specific surface area, S_{CO} (m^2 g_{Pt}^{-1}) was calculated from the CO oxidation peak current, assuming that the electrooxidation of a full monolayer of CO_{ad} requires 420×10^{-2} C m_{Pt}^{-2} [39]. The CO equivalent particle diameter, d_{CO}, was calculated from CO stripping results by [36–38]:

$$d_{CO} = \frac{6 \times 10^{-3}}{\rho_{Pt} S_{CO}} \quad (4)$$

where ρ_{Pt} is the density of Pt (21.4×10^3 kg m^{-3}). As CO stripping voltammetry is a surface-sensitive method, d_{CO} corresponds to a surface weighed average diameter and can be compared to d_s.

Activity for the oxygen reduction reaction. The activity of the catalysts for the oxygen reduction reaction (ORR) was measured on a rotating disk electrode (RDE). After saturation of the electrolyte by oxygen bubbling during 15 min, the electrode potential was set at 0.4 V *vs.* NHE, then increased at 2 mV s^{-1} to 1.09 V *vs.* NHE and finally decreased back to 0.4 V *vs.* NHE at the same scan rate, while measuring the reduction current. This measurement was repeated at various rotation speeds of the electrode (400, 900, 1600, and 2500 rpm). For each rotation speed of the electrode, the kinetic current was calculated by correcting the measured current for the effect of the external mass transfer limitations in the solution using the Koutecky–Levich equation [40]:

$$\frac{1}{i_k} = \frac{1}{i} - \frac{1}{i_{l,c}} \quad (5)$$

Table 3
Properties determined by physicochemical analyses of catalysts synthesized *via* multiple impregnation-reduction cycles.

Catalyst	Pt_{ICP} (wt.%) ± 0.1	d_{TEM} (nm)	σ (nm)	d_s (nm)	d_v (nm)	d_{XRD} (nm) ± 0.5
SEA/1	8.4	2.3	0.7	2.7	2.9	2.6
SEA/2	14.7	2.2	0.7	2.7	3.0	2.3
SEA/3	19.0	2.1	0.6	2.5	2.7	2.5
SEA/4	22.2	2.2	0.7	2.6	2.8	2.4
SEA/5	25.3	2.1	0.7	2.6	2.8	2.6
CEDI/1	7.7	1.6	0.4	1.8	1.9	–[a]
CEDI/2	14.0	2.6	2.1	6.4	8.2	4.6
CEDI/3	19.7	2.9	2.6	7.6	9.2	4.6
CEDI/4	24.8	3.2	2.1	6.1	7.5	4.6
CEDI723/1	7.8	1.3	0.4	1.6	1.7	–[a]
CEDI723/2	13.9	1.9	1.5	5.2	7.2	6.4
CEDI723/3	19.9	2.4	1.9	6.2	8.2	7.3
CEDI723/4	24.6	2.6	1.9	5.6	6.9	7.3
SB/2	10.4	3.0	1.3	4.2	5.3	3.7
SB/4	15.6	2.8	1.8	5.1	6.1	4.1
SB/6	19.4	3.0	1.5	4.5	5.3	4.4
SB/8	23.1	4.8	4.4	14.6	20.5	4.4
SB723/2	11.0	3.8	2.5	7.3	9.2	11.0
SB723/4	16.1	4.8	4.3	15.9	24.1	12.8
SB723/6	20.3	3.8	4.9	28.4	47.1	22.0
SB723/8	23.9	4.3	4.3	13.9	18.3	22.0
Ref	37.0	3.1	0.8	3.4	3.6	2.4[b]

Pt_{ICP}: Pt weight percentage of the catalyst measured by ICP-AES; d_{TEM}: average diameter of the particles estimated from TEM micrographs; σ: standard deviation associated with d_{TEM}; d_s: surface-weighed average diameter of particles estimated from TEM micrographs and calculated by Eq. (1); d_v: volume-weighed average diameter of particles estimated from TEM micrographs and calculated by Eq. (2); d_{XRD}: average size of crystallites calculated from X-ray diffraction peaks *via* Eq. (3).

[a] No Pt peak is visible.

[b] Large error (± 1) due to low intensity of diffraction peaks.

where i_k is the kinetic current, *i.e.* the current without any mass transfer limitations, i is the experimental current, and $i_{l,c}$ is the cathodic limit current, which depends on the rotation speed of the electrode. The values of this averaged kinetic current at 0.9 V *vs.* RHE were divided by the electroactive surface of the catalysts in order to obtain the specific activity of the catalysts at 0.9 V *vs.* RHE, *SA* (in A m_{Pt}^{-2}), or divided by the mass of Pt deposited on the electrode in order to obtain the mass activity at 0.9 V *vs.* RHE, *MA* (in A g_{Pt}^{-1}).

3. Results

3.1. Physicochemical characterization

The physicochemical properties of the catalysts synthesized *via* multiple impregnation-reduction cycles are summarized in Table 3; those of the catalysts synthesized *via* one-step deposition methods are summarized in Table 4. In each case, the results are compared to those of the reference catalyst, Ref.

Fig. 1 shows the TEM micrographs of the catalysts with the lowest and the highest loading for each synthesis technique (SEA, CEDI, multiple SB reduction, one-step SB reduction, *i.e.* SB-20, and the other one-step techniques *i.e.* FA and Col) and the TEM micrograph of the Ref catalyst. Pt particle size distribution (PSD) histograms of all the catalysts are shown in Fig. 2.

X-ray diffractograms of the series of catalysts are presented in Fig. 3. The Ref diffractogram, which is present in every XRD figure, is used for comparison. Almost every diffractogram displays two diffraction peaks: one at an angle of 39.7° and another at an angle of 46.2°, corresponding to Pt (1 1 1) and Pt (2 0 0) facets, respectively.

Table 4
Properties determined by physicochemical analyses of catalysts synthesized *via* one-step deposition methods.

Catalyst	Pt_{target} wt.%	Pt_{ICP} (wt.%) ± 0.1	d_{TEM} (nm)	σ (nm)	d_s (nm)	d_v (nm)	d_{XRD} (nm) ± 0.5
SB-20	20	17.5	4.1	3.3	12.9	19.7	4.1
FA-10	10	10.2	2.8	1.0	3.8	5.2	2.6
FA-20	20	16.5	3.6	1.0	4.2	4.6	2.9
FA-30	30	22.7	3.6	1.5	5.8	9.7	2.9
FA-40	40	37.0	3.6	1.2	5.0	8.1	2.9
Col-10	10	5.2	2.8	1.9	4.8	7.3	3.7[a]
Col-20	20	15.6	2.9	1.7	6.0	8.8	2.7
Col-30	30	15.4	3.0	1.3	4.4	5.7	2.6
Col-40	40	25.2	3.7	1.7	5.4	6.4	3.1
Ref	–[b]	37.0	3.1	0.8	3.4	3.6	2.4[a]

Pt_{target}: Pt loading targeted by the one-step deposition synthesis; Pt_{ICP}: Pt weight percentage of the catalyst measured by ICP-AES; d_{TEM}: average diameter of the particles estimated from TEM micrographs; σ: standard deviation associated with d_{TEM}; d_s: surface-weighed average diameter of particles estimated from TEM micrographs and calculated by Eq. (1); d_v: volume-weighed average diameter of particles estimated from TEM micrographs and calculated by Eq. (2); d_{XRD}: average size of crystallites calculated from X-ray diffraction peaks *via* Eq. (3).

[a] Large error (± 1) due to low intensity of diffraction peaks.

[b] Not pertinent (commercial catalyst).

3.2. Electrochemical characterization

The Pt specific surface area, S_{CO}, and the CO equivalent particle diameter of Pt particles, d_{CO}, were calculated from the CO stripping voltammograms (Fig. 4). Results are in each case compared to those obtained with the reference catalyst, Ref. The values of these parameters are gathered in Table 5. The catalytic activity of the catalysts were compared using the specific activity, *SA*, and the mass activity, *MA*, measured at 0.9 V *vs.* NHE (Table 5). An example of ORR experiment, performed at four different rotating speeds (400, 900, 1600, and 2500 rpm), is shown in SI (Fig. SI.1). All the measurements were performed at least twice to check for the reproducibility; Fig. SI.2, displayed in SI, shows two Tafel plots obtained from consecutive ORR characterizations on the same sample (CEDI723/4).

3.3. Strong electrostatic adsorption

The results obtained by SEA are in agreement with previous works [27,22]. To sum up, the SEA method allows obtaining well-distributed Pt over the CX support with high weight percentages up to 25.3 wt.% (SEA/5, Table 3) and average particle size, d_{TEM}, around 2.2 nm. Nevertheless, the amount of Pt deposited decreases with the number of steps. The catalysts also display d_{CO} around 2.9 nm, which has to be compared to d_s (2.6 nm), and d_{XRD} around 2.5 nm which can be compared to d_v (2.8 nm). All the values of average particle sizes for SEA-synthesized catalysts are close to each other and the standard deviation calculated by image analysis is very low, equal to 0.6–0.7 nm. In fact, the PSD of the SEA-synthesized catalysts are the same for the five catalysts (Fig. 2a). Moreover, the Pt specific surface area is constant (92–96 $m^2\ g_{Pt}^{-1}$, Table 5) as well as the specific and the mass activity (*SA* from 0.09 to 0.11 A m_{Pt}^{-2} and *MA* ranging from 8.6 to 10.5 A g_{Pt}^{-1}). These results indicate that the Pt deposited at each impregnation-reduction step only forms new particles with the same size and the same activity as the previously deposited particles. It must be noted that the SEA catalysts were reduced under H_2 at high temperature (723 K), ensuring the removal of Cl ions from the Pt particle surface.

3.4. Charge enhanced dry impregnation

The first Pt deposition using the CEDI method allows to synthesize small, well-dispersed Pt particles (d_{TEM} equal to 1.6 nm with a standard deviation of 0.4 nm, see the PSD in Fig. 2b) and a Pt loading of 7.7 wt.% (CEDI/1, Table 3). These particles are too small to induce X-ray diffraction peaks, as no peak is visible on the X-ray diffractogram (Fig. 3b). The observed diffractogram corresponds to the background due to the CX support (very broad diffraction peak around 40°). However, the small Pt particles can be seen on the TEM micrograph (Fig. 1c). Concerning the electrochemical properties, the CO stripping voltammogram displays a small, broad peak around 1.0 V *vs.* NHE (Fig. 4b), representative of small particles. The S_{CO} of CEDI/1 is low (50 $m^2\ g_{Pt}^{-1}$) as well as the *MA* (3.6 A g_{Pt}^{-1}) and with *SA* slightly lower than that of the reference catalyst (0.072 A m_{Pt}^{-2} compared to 0.091 A m_{Pt}^{-2}, Table 5). The low S_{CO} value, with regard to the size of particles (*ca.* 1–2 nm, which should correspond to a surface of at least 100 $m^2\ g_{Pt}^{-1}$) is certainly due to Cl poisoning the surface, as explained in the paragraphs below. This also explains the low *MA* value. These results are consistent with those obtained by Cao et al. [28].

The second to fourth Pt deposition steps increase the loading up to 24.8 wt.% (after four impregnation-reduction cycles). However, the Pt PSD does not remain the same (Fig. 2b), as d_{TEM} increases from 1.6 nm (CEDI/1) to 3.2 nm (CEDI/4) (Table 3). Moreover, the standard deviation increases from 0.4 to 2.6 nm. These results indicate that, during impregnation, all the Pt ions do not adsorb on the CX support to form new particles (same mechanism as for the SEA synthesis). Indeed, particles of different sizes can be seen on the TEM micrograph (Fig. 1d). This may be due to the fact that the CX surface chemistry is modified during the impregnation-reduction cycles. Indeed, the Pt uptake may be lowered by the modification of the CX surface chemistry. This decrease in Pt uptake with the succession of impregnation-reduction cycles has already been observed in the case of the multiple SEA method [22]. As the excess Pt ions are not withdrawn by filtration (like in SEA synthesis), Pt ions stay in the solution filling the CX pores. Therefore, during the drying step, they may adsorb on the available CX surface or agglomerate with other Pt ions, the latter producing larger nanoparticles.

X-ray diffractograms (Fig. 3b), show sharp diffraction peaks, which results in relatively large d_{XRD} values (4.6 nm for the three multi-impregnated samples, CEDI/2, CEDI/3 and CEDI/4). However, deep analysis of the diffractograms show that they are composed of one sharp peak due to large crystallites and one broad peak due to the presence of smaller crystallites. This hints at the heterogeneity of the particle size. Regarding the electrochemical properties, the CO stripping voltammograms are composed of two very small peaks, one small, broad peak at high potential (from 0.9 to 1.1 V *vs.* NHE) due to particles with low diameters (lower than 3 nm), and one small, sharp peak at lower potential (0.85 V *vs.* NHE) due to particles with diameters higher than 3 nm [36]. Consequently, S_{CO} remains low (*ca.* 30 $m^2\ g_{Pt}^{-1}$) leading to high d_{CO} of *ca.* 8 nm (Table 5) which does not match the d_s values (from 6.1 to 7.6 nm). The specific activities, *SA*, of CEDI/2, CEDI/3, and CEDI/4 are the highest, up to a value of 0.183 A m_{Pt}^{-2} for CEDI/4. Notwithstanding the high *SA* values, the mass activities, *MA*, of these catalysts are the lowest with a value around 6 A g_{Pt}^{-1}.

These catalysts underwent a 5 h reduction at 723 K under H_2, becoming the CEDI723 catalysts. The high temperature reduction does not affect the PSD much, even though the curves are slightly narrower (Fig. 2c), as d_{TEM}, σ, d_s, and d_v of CEDI723 catalysts are slightly lower than those of CEDI catalysts (Table 3). This result could be due to the sampling of the TEM micrographs (Fig. 1c and e, and Fig. 1d and f). However, the average crystallite size, d_{XRD} increases from 4.6 nm to 6.4 nm for CEDI723/2 or to 7.3 nm for CEDI723/3 and CEDI723/4 as the X-ray diffraction peaks gets sharper (Fig. 3c). Nonetheless, the high temperature reduction has more significant impact on the electrochemical properties. Indeed, the CO stripping voltammograms (Fig. 4c) exhibit one large peak at 0.95 V *vs.* NHE for CEDI723/1, one large peak at 0.9 V *vs.* NHE with a shouldering around 0.85 V *vs.* NHE for CEDI723/2 and CEDI723/3, and one large peak at 1 V *vs.* NHE with a shouldering around 0.85 V *vs.* NHE for CEDI723/4. The CO stripping

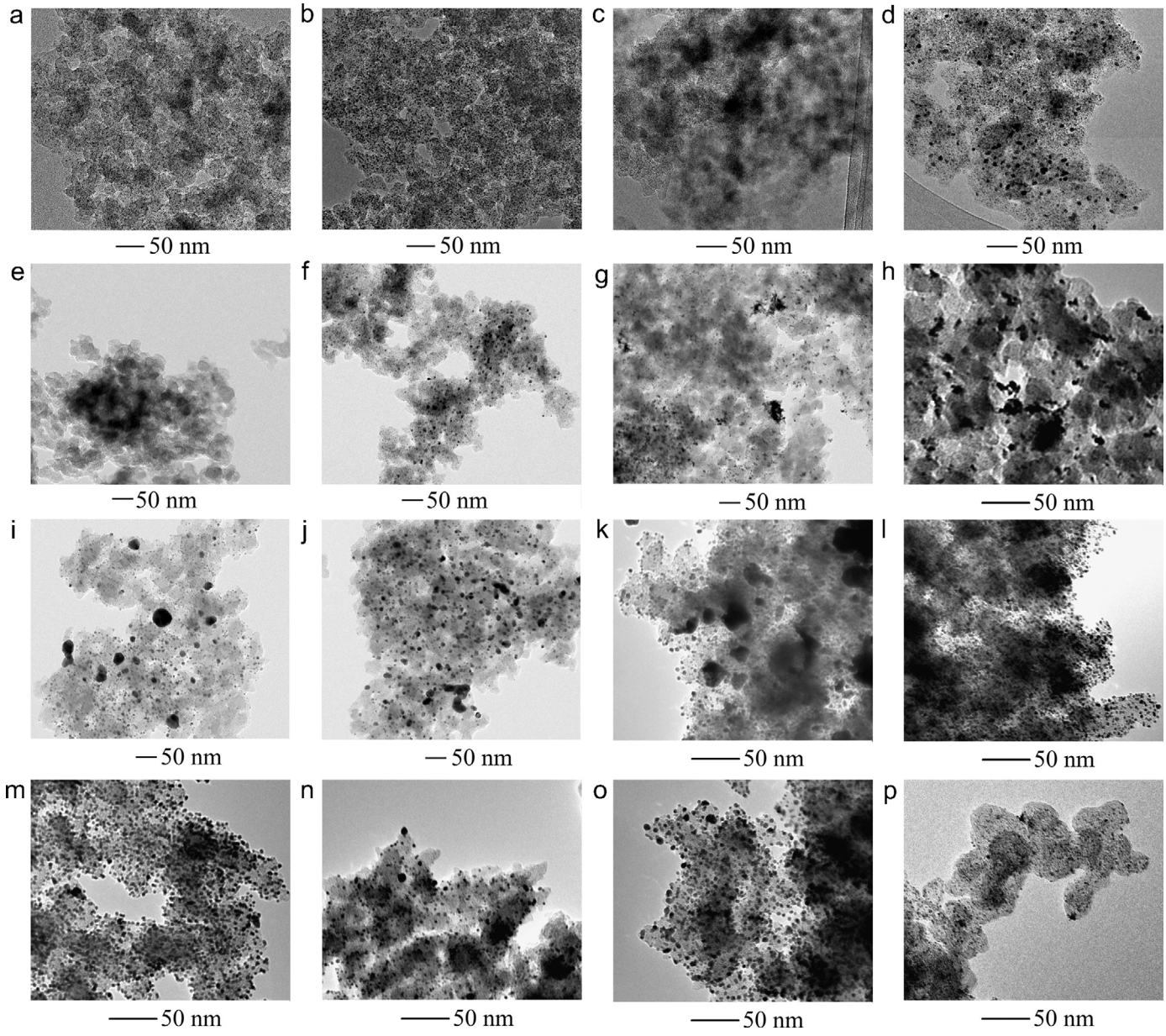

Fig. 1. TEM micrographs of the catalysts with the lowest and the highest loading for each synthesis and the commercial catalyst: SEA/1 (a), SEA/5 (b), CEDI/1 (c), CEDI/4 (d), CEDI723/1 (e), CEDI723/4 (f), SB/2 (g), SB/8 (h), SB723/2 (i), SB723/8 (j), SB-20 (k), FA-10 (l), FA-40 (m), Col-10 (n), Col-40 (o), and Ref (p).

peak of CEDI723/1 is representative of Pt particles with diameter lower than 3 nm [36], which is consistent with the TEM micrograph (Fig. 1e). Moreover, S_{CO} of CEDI723/1 is huge (247 $m^2\ g_{Pt}{}^{-1}$) leading to very small d_{CO} (1.1 nm). The large CO stripping peaks of the other three CEDI723 catalysts are due to Pt particles with diameters lower than 3 nm, while the shoulderings are due to Pt particles with diameters higher than 3 nm [36]. These larger Pt particle sizes induce S_{CO} values lower than that of CEDI723/1 (from 130 to 190 $m^2\ g_{Pt}{}^{-1}$ instead of 250 $m^2\ g_{Pt}{}^{-1}$). Surface areas are still very high, leading to small d_{CO} values (1.4–2.1 nm).

When comparing d_{CO} and d_s of the CEDI and the CEDI723 catalysts, one can see that d_{CO} is always higher than d_s for the CEDI catalysts and always lower than d_s for the CEDI723 catalysts. The only difference between these two series of catalysts is the last reduction step, which is performed at higher temperature and for longer time (723 K for 5 h) in the case of the CEDI723 catalysts. For the CEDI catalysts, the cause of the difference between d_{CO} and d_s is the presence of Cl poisoning the surface. Indeed, as Cl can only be removed with high temperature reduction treatment [27], the small nanoparticles are still poisoned by Cl. These small and poisoned nanoparticles are not detected by CO stripping measurements, leading to a decrease in the Pt electroactive surface, *i.e.* to an increase in d_{CO}. For the CEDI723 catalysts, the cause of the difference between d_{CO} and d_s is the presence of large nanoparticles detected by TEM. Indeed, large nanoparticles heavily impact on d_s values as the presence of a few large nanoparticles greatly increases d_s values. Concerning the electrochemical activities, the *SA* values of the CEDI catalysts are high because most of the small particles, with low activity surface atoms, are covered with Cl, as shown by the low S_{CO} values. Indeed, Cl is more strongly bonded on small Pt particles than at the surface of larger ones [33]. On the contrary, upon reduction under H_2 at high temperature (CEDI723 catalysts), Cl is removed from the small particles; this leads to higher S_{CO} values, and lower *SA*, since the Pt surface atoms of small particles are much less active. These results prove that the high temperature reduction impacts the catalysts properties by two major effects: on the one hand, the high temperature increases the crystallite size by sintering the least stable Pt

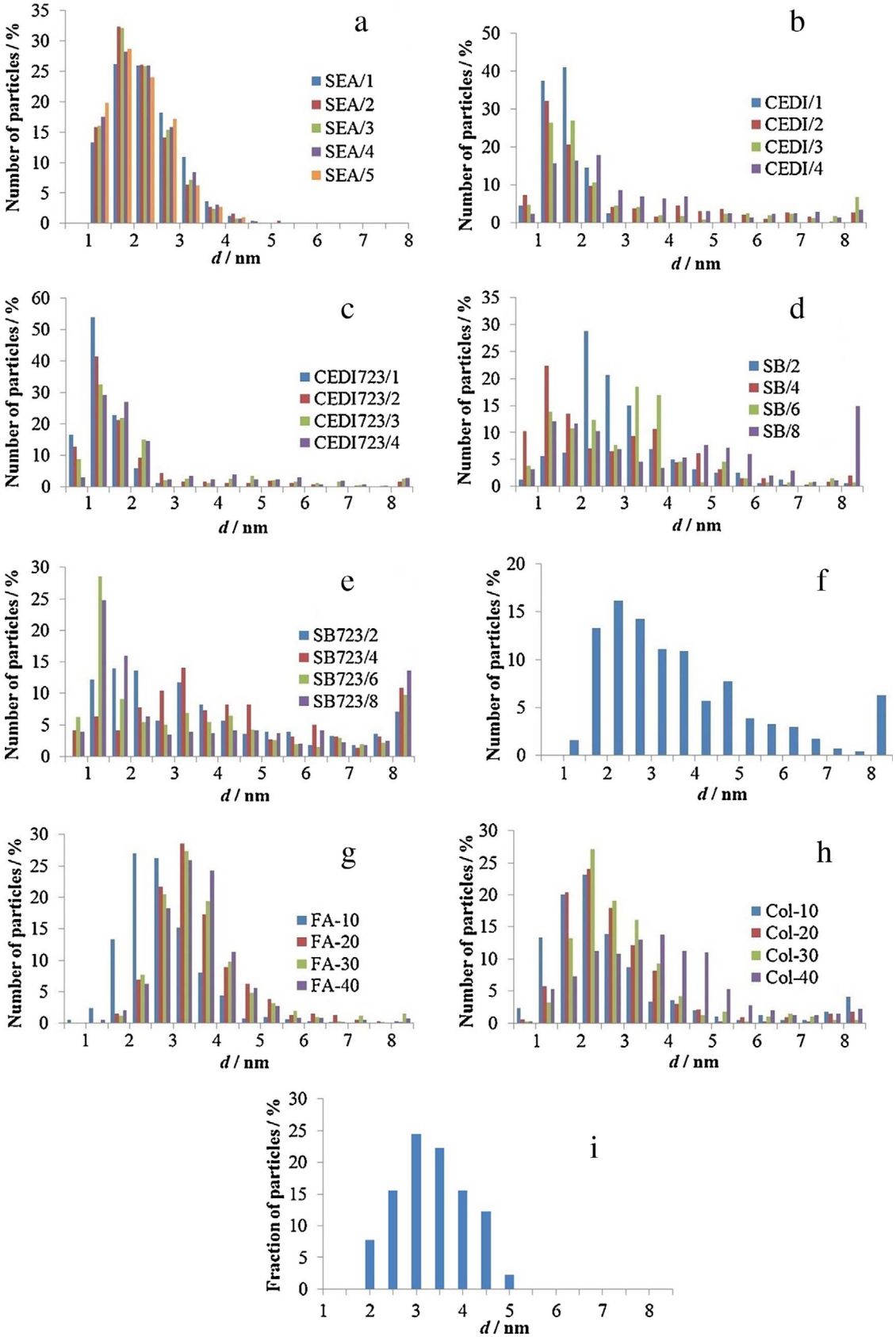

Fig. 2. Pt particle size distribution histograms of all the catalysts obtained by image analysis: SEA/1 to SEA/5 (a); CEDI/1 to CEDI/4 (b); CEDI723/1 to CEDI723/4 (c); SB/2 to SB/8 (d); SB723/2 to SB723/8 (e); SB-20 (f); FA-10 to FA-40 (g); Col-10 to Col-40 (h); and of the reference catalyst, Ref (i). The last category of the histograms represents the fraction of Pt particles with diameter higher than 8 nm.

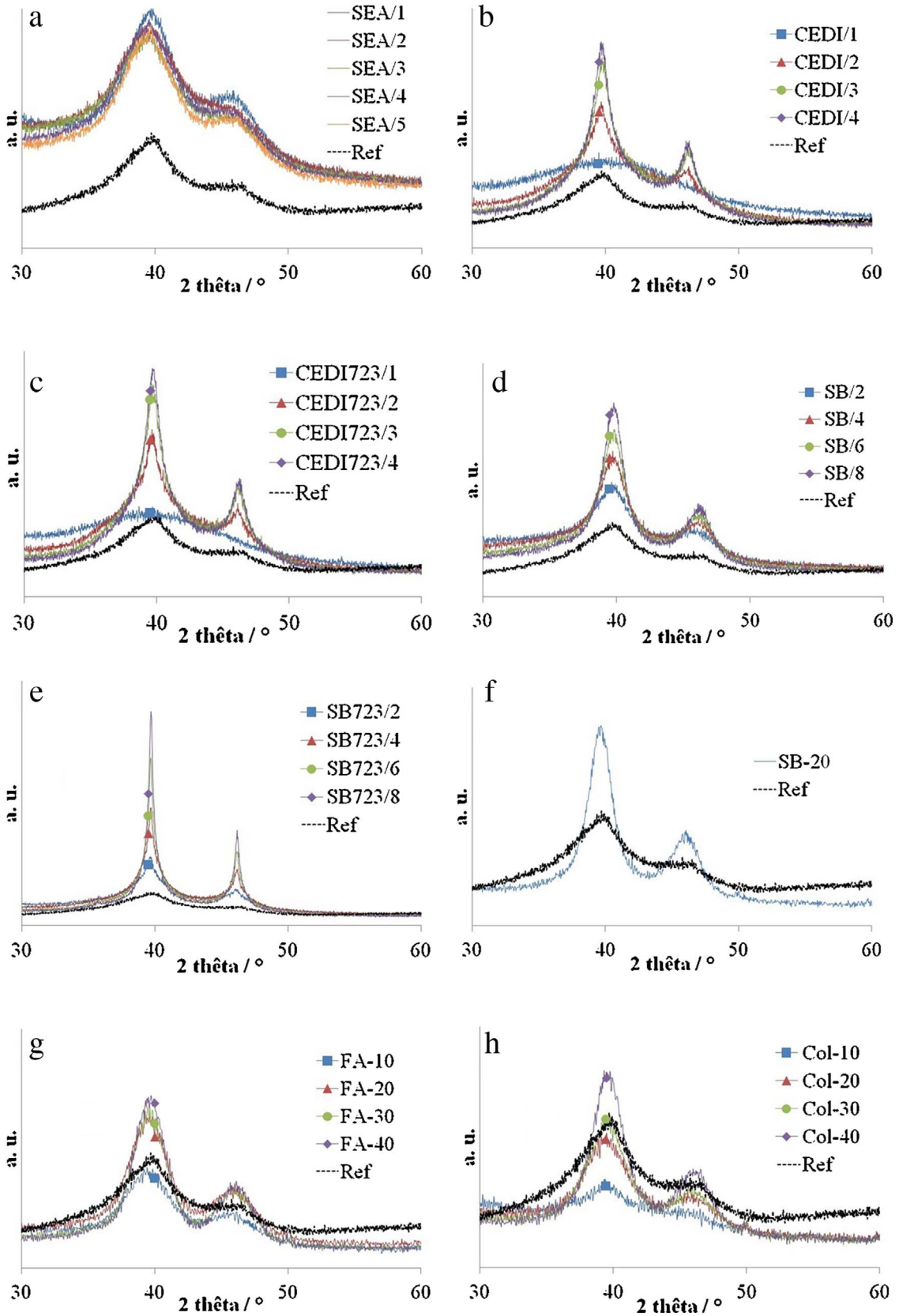

Fig. 3. XRD diffractograms of all the catalysts: SEA/1 to SEA/5 (a); CEDI/1 to CEDI/4 (b); CEDI723/1 to CEDI723/4 (c); SB/2 to SB/8 (d); SB723/2 to SB723/8 (e); SB-20 (f); FA-10 to FA-40 (g); Col-10 to Col-40 (h). The Ref diffractogram (dotted black line) serves as a basis for comparison.

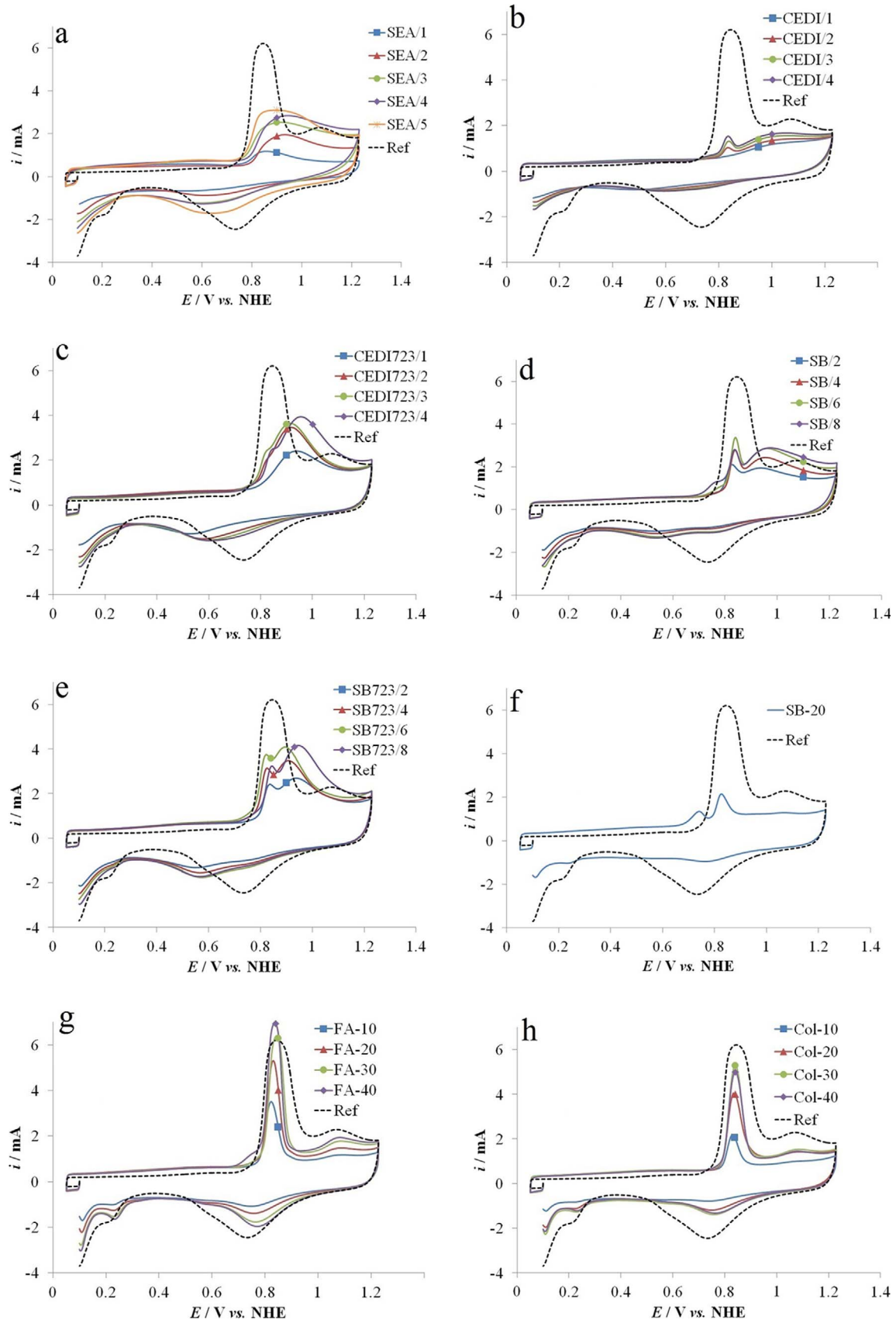

Fig. 4. CO electrooxidation voltammograms of all the catalysts in 1 M H_2SO_4 at a sweep rate of 20 mV s^{-1} at room temperature: SEA/1 to SEA/5 (a); CEDI/1 to CEDI/4 (b); CEDI723/1 to CEDI723/4 (c); SB/2 to SB/8 (d); SB723/2 to SB723/8 (e); SB-20 (f); FA-10 to FA-40 (g); Col-10 to Col-40 (h). The voltammogram of the Ref sample (dotted line) is reported in each case for comparison.

Table 5
Properties determined by electrochemical analyses of all the catalysts.

Catalyst	S_{CO} ($m^2\ g_{Pt}^{-1}$) ± 10%	d_{CO} (nm) ± 10%	*SA* ($A\ m_{Pt}^{-2}$) ± 10%	*MA* ($A\ g_{Pt}^{-1}$) ± 10%
SEA/1	92	3.0	0.114	10.5
SEA/2	93	3.0	0.093	8.6
SEA/3	94	2.9	0.102	9.6
SEA/4	96	2.9	0.093	8.9
SEA/5	96	2.9	0.105	10.1
CEDI/1	50	5.5	0.072	3.6
CEDI/2	38	7.2	0.147	5.6
CEDI/3	34	8.0	0.177	6.0
CEDI/4	31	8.8	0.183	5.7
CEDI723/1	247	1.1	0.030	7.4
CEDI723/2	193	1.4	0.056	10.8
CEDI723/3	145	1.9	0.065	9.4
CEDI723/4	130	2.1	0.083	10.0
SB/2	171	1.6	0.044	7.5
SB/4	133	2.1	0.050	6.7
SB/6	115	2.4	0.047	5.4
SB/8	92	3.0	0.097	8.9
SB723/2	209	1.3	0.042	8.8
SB723/4	167	1.6	0.044	8.4
SB723/6	152	1.8	0.059	9.0
SB723/8	129	2.1	0.051	6.6
SB-20	73	3.8	0.121	8.8
FA-10	131	2.1	0.086	11.3
FA-20	113	2.4	0.103	11.6
FA-30	92	3.0	0.109	10.0
FA-40	59	4.7	0.138	8.1
Col-10	137	2.0	0.069	9.5
Col-20	99	2.8	0.064	6.3
Col-30	111	2.5	0.065	7.2
Col-40	61	4.5	0.099	6.0
Ref	91	3.0	0.091	8.2

S_{CO}: Pt specific surface area calculated from CO stripping measurements normalized by the mass of Pt on the electrode; d_{CO}: CO equivalent particle diameter of the Pt particles calculated by Eq. (4); *SA*: ORR specific activity measured at 0.9 V *vs.* NHE; *MA*: ORR mass activity measured at 0.9 V *vs.* NHE.

particles; on the other hand, the high temperature reduction cleans the Pt surface from the strongly-adsorbed chlorine, allowing to measure the actual Pt specific surface area [33].

3.5. Sodium borohydride reduction

When reducing Pt ions with SB, the impregnation-reduction cycle must be repeated eight times in order to reach a Pt loading of 23.9 wt. %. Despite the higher number of impregnation-reduction steps, the SB reduction synthesis is faster than other multiple impregnation-reduction steps methods. Indeed, as both impregnation and reduction occur in liquid phase, the drying step between each cycle becomes superfluous. In that way, one impregnation-reduction cycle requires only 1.5 h.

The lower deposited Pt amount per round may be due to a desorption of Pt ions when suspending the CX in ultrapure water after the impregnation step. This step is however needed in order to proceed with the SB reduction in liquid phase. Even if the pH was fixed at the optimal pH, some ions can desorb to yield an equilibrium between the adsorbed and the desorbed Pt ions. These desorbed ions could be reduced to form Pt particles without any bonds to the CX surface. Part of them could be washed away during rinsing, decreasing the amount of deposited Pt. The other part could deposit on the CX surface. As the size of these reduced-when-desorbed particles was not controlled, the average particle size, d_{TEM}, is higher than that of the previous catalysts (around 3 nm, Table 3), and the PSD wider (Fig. 2d), as σ values are high. Large Pt particles are clearly visible on the TEM micrographs (Fig. 1g and h: particles from 1 nm up to more than 10 nm). Moreover, some aggregates can be seen. This discrepancy in Pt particle size makes difficult the comparison between the different measurement methods (TEM, XRD, CO stripping). X-ray diffraction peaks are sharp (Fig. 3d), which results in a relatively high d_{XRD} of *ca.* 4 nm for the four SB catalysts. The CO stripping voltammograms (Fig. 4d) show two peaks for the four SB catalysts: one broad peak around 1 V *vs.* NHE, representative of particles with diameter lower than 3 nm, and one sharp peak around 0.85 V *vs.* NHE, representative of particles larger than 3 nm [36]. The fact that the small, chlorine-poisoned Pt particles can be detected by CO stripping measurements without any high temperature reductions may be due to the reductive strength of SB, which can remove a large part of the chlorine covering the Pt surface. Moreover, a shouldering appears starting from the sixth Pt deposition (SB/6) at around 0.75 V *vs.* NHE, representative of Pt particles aggregates [37]. S_{CO} exhibits high values ranging from 92 to 171 $m^2\ g_{Pt}^{-1}$, leading to small d_{CO} values ranging from 1.6 to 3.0 nm. It seems that the wide PSDs stem from two reduction mechanisms: (i) some Pt ions are reduced after adsorption on the CX support, leading to small particles, and (ii) some other Pt ions are reduced in liquid phase and then deposited on the CX surface, leading to larger particles [30]. The phenomenon seems to worsen with the number of Pt deposition steps (see the physicochemical properties of SB/8 in Table 3 and the PSD in Fig. 2d). The SB reduction at room temperature is probably too quick to control the Pt particle size. Concerning the activities, the *SA* of these catalysts are low (around 0.050 $A\ m_{Pt}^{-2}$) except for SB/8 (0.097 $A\ m_{Pt}^{-2}$) but, despite the high S_{CO} values, *MA* values remain relatively low (from 5.4 to 8.9 $A\ g_{Pt}^{-1}$).

The SB catalysts were also reduced at 723 K during 5 h, becoming the SB723 series. After that treatment, the Pt particle size increases and previously-formed aggregates sinter to form very large particles of several tens of nm (Table 3, Figs. 1i, j and 2e). Fig. 3e displays the sharpest X-ray diffraction peaks of this study, and so the SB723 catalysts exhibit the higher d_{XRD} with values up to 22 nm. This indicates that the high temperature reduction induces Pt particles sintering. In the CO stripping voltammograms (Fig. 4e), two oxidation peaks are visible: one broad peak around 0.9 V *vs.* NHE representative of particles with diameter lower than 3 nm and one sharp peak around 0.85 V *vs.* NHE representative of particles with diameter higher than 3 nm. The areas under these peaks are higher than those of SB catalysts, especially for the peaks representative of small particles, most certainly because of the particle surface cleaning from Cl which occurs during the high temperature reduction. The third oxidation peak, appearing at around 0.75 V *vs.* NHE and attributed to aggregates, can no longer be seen. It seems that the aggregates sinter in large monocrystalline particles during the high temperature reduction. Therefore, as the contribution of large particles is integrated in the second oxidation peak around 0.85 V *vs.* NHE, the third peak tends to decrease or disappear. The S_{CO} of the SB723 catalysts are high with values ranging from 129 to 209 $m^2\ g_{Pt}^{-1}$ for SB723/8 and SB723/2 respectively. So, d_{CO} is low, around 2 nm. Regarding catalytic activities, SB723 catalysts display low *SA ca.* 0.04–0.05 $A\ m_{Pt}^{-2}$ and high *MA ca.* 8 $A\ g_{Pt}^{-1}$. These results seem to indicate that the SB723 catalysts are mainly constituted of very small, clean particles (2 nm and lower, without Cl at the surface). They also contain some large particles which seem to have low impact on the properties. The further cleaning of the Pt particle surface suggests that, even if the SB reduction partly cleans the Pt surface, it is not as effective as reduction under H_2 at high temperature.

Results obtained for the SB-20 catalyst are similar to those obtained for other SB-reduced catalysts. The Pt loading is close to the target of 20 wt.% (17.5 wt.%, Table 4) but the Pt PSD is wider (d_{TEM} equal to 4.1 nm, σ equal to 3.3 nm, see Fig. 2f). The presence of small (around 2 nm) and huge (several tens of nm) nanoparticles can also be seen on TEM micrograph (Fig. 1k). The X-ray diffractogram (Fig. 3f) is similar to those of SB catalysts and the value of d_{XRD} is in the same range (equal to 4.1 nm), indicating that the large particles detected by TEM

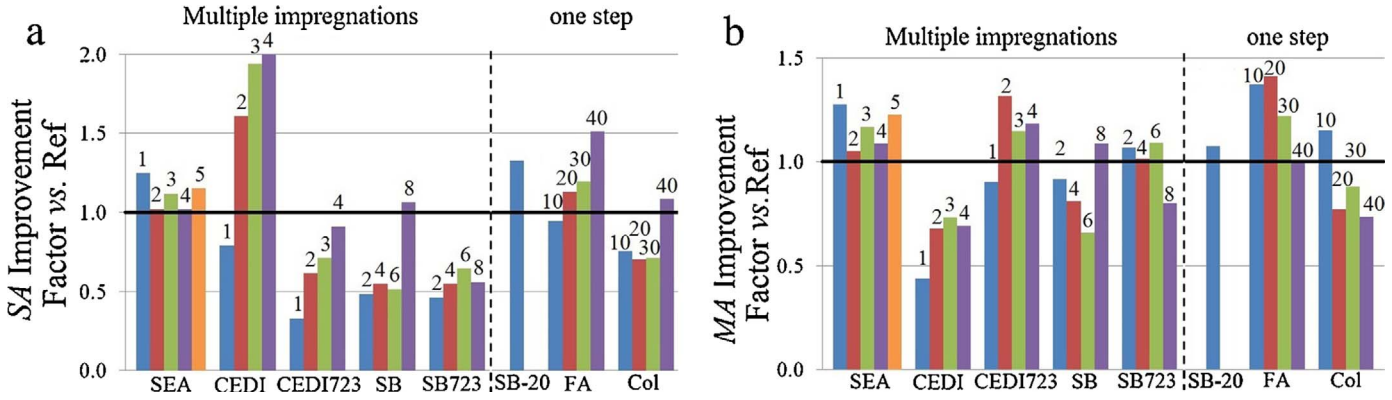

Fig. 5. *SA* (a) and *MA* (b) improvement factor *vs.* Ref. The horizontal black line represents improvement factor of 1, *i.e.* the position of the reference (commercial catalyst, Ref). The number upon each bar represents the number of impregnations the catalyst underwent (in the case of multiple impregnations methods) or the targeted loading (in the case of one-step methods).

measurements may be aggregates as no large crystallites are detected. In the CO stripping voltammogram, no oxidation peak representative of small particles (lower than 3.3 nm), at high potential around 1 V *vs.* NHE, is visible. Again, this is probably due to the Cl poisoning. However, the curve exhibits two other peaks: one at 0.85 V *vs.* NHE, representative of particles with diameter higher than 3.3 nm, and the other at 0.75 V *vs.* NHE, representative of aggregates. SB-20 displays a small S_{CO} value (73 $m^2\ g_{Pt}^{-1}$) and a high d_{CO} value (3.8 nm). However, *SA* and *MA* of SB-20 catalyst are higher than in the case of Ref (0.121 A m_{Pt}^{-2} and 8.8 A g_{Pt}^{-1}, respectively, Table 5). These electrochemical measurements show that the Pt surface is not clean: Cl species that may be removed *via* high temperature reduction, are much probably still present on the Pt surface like in the case of previous catalysts (CEDI and SB series). The pertinence of the high temperature reduction will be debated in the Discussion section.

3.6. Formic acid reduction

Concerning the Pt loading values, measured by ICP-AES (Table 4), the targeted loadings are almost reached in each case, except for sample FA-30, which displays a lower Pt loading (22.7 wt.% instead of 30 wt. %). This difference, probably a mishap as FA-40 did not suffer from the same problem, may be due to the detachment of some Pt particles with low interactions with the CX support during the filtration and/or the washing. d_{TEM} is equal to 2.8 nm for FA-10 and to 3.6 nm for the other three FA catalysts. All FA catalysts display low σ, d_s, and d_v, as the PSDs are narrow (Fig. 2g). Moreover, in Fig. 1l and m, it can be seen that all the Pt particles are well distributed without any large particles or aggregates. In Fig. 3g, the X-ray diffractograms exhibit broad Pt diffraction peaks, representative of small Pt particles. Furthermore, d_{XRD} is constant for the four FA catalysts (2.6 nm for FA-10 and 2.9 nm for the others). In the CO stripping voltammograms (Fig. 4g), the four FA catalysts display a CO oxidation peak at 0.85 V *vs.* NHE. This peak is representative of particles with diameters higher than 3.3 nm [36]. Only the FA-40 catalyst exhibits a shouldering at 0.75 V *vs.* NHE, indicating that some aggregates are present (not visible in Fig. 1m). Both the peak area and the peak height increase with the Pt loading. S_{CO} is high for FA-10 (131 $m^2\ g_{Pt}^{-1}$) and decreases to 59 $m^2\ g_{Pt}^{-1}$ when increasing the loading up to 37 wt.% (FA-40). In parallel, d_{CO} increases from 2.1 nm (FA-10) to 4.7 nm (FA-40). The values of *SA* are high and increase with the Pt loading from 0.086 to 0.138 A m_{Pt}^{-2}. The values of *MA* are high but they decrease with the Pt loading, from 11.3 to 8.1 A g_{Pt}^{-1}.

3.7. Colloid synthesis

In Table 4, it can be seen that the targeted Pt loading is not reached, whatever the sample. The highest loading value equals 25.2 wt.% (Col-40). The reasons are probably that all the Pt particles in the colloid suspension did not deposit on the CX support during the mixing and that some Pt particles could be washed off. Concerning the Pt particle size, the values of d_{TEM} are quite low and increase with the targeted Pt loading, from 2.8 to 3.7 nm. The Pt PSDs are relatively wide (Fig. 2h), which leads to large values of σ, d_s, and d_v. This may be due to the presence in solution of both tSC, which is a weak reductant, and SB, a strongly active reductant. Indeed, as Pt is easily reducible, it can be reduced by both reductants, leading to more dispersed PSD, *i.e.* to small and large Pt particles. However, no large particles or aggregates are visible. X-ray diffraction corroborates the small particle size as detected peaks are broad. d_{XRD} values calculated from these peaks are low (*ca.* 3 nm), except for Col-10 (3.7 nm). However, this is certainly due to the accuracy, as the diffraction peaks are very small. The four CO stripping voltammograms exhibit a CO oxidation peak at 0.85 V *vs.* NHE (Fig. 4h). The peak area and height increase with the Pt loading. This peak is representative of particles with diameter higher than 3.3 nm. S_{CO} is high (values between 99 and 137 $m^2\ g_{Pt}^{-1}$ for Col-20 and Col-10 respectively) and d_{CO} is low (between 2 and 3 nm), except Col-40 (S_{CO} equal to 61 $m^2\ g_{Pt}^{-1}$, d_{CO} equal to 4.5 nm). The values of *SA* are low, around 0.065 A m_{Pt}^{-2}, except for Col-40 (0.099 A m_{Pt}^{-2}). Furthermore, the values of *MA* are low, *ca.* 6.5 A g_{Pt}^{-1}, except for Col-10 which displays a *MA* value equal to 9.5 A g_{Pt}^{-1}. This high *MA* value is due to the high S_{CO} value of Col-10 (137 $m^2\ g_{Pt}^{-1}$). Col-10, Col-20, and Col-30 catalysts display Pt particles around the same size, as shown by TEM results, CO stripping results, and identical *SA* values. However, Col-40 catalyst displays larger Pt particles than other Col catalysts, as proved by TEM results, CO stripping results, and higher *SA*.

4. Discussion

The electrochemical properties of the catalysts synthesized in this work were compared to those of a reference, the commercial catalyst Tanaka containing 37 wt.% of Pt, labeled hereafter Ref. This commercial catalyst exhibits the following parameters: S_{CO} equal to 91 $m^2\ g_{Pt}^{-1}$, d_{CO} equal to 3.0 nm, *SA* equal to 0.091 A m_{Pt}^{-2}, and *MA* equal to 8.2 A g_{Pt}^{-1} (Table 5). Concerning the Pt loading, every synthesized catalyst displays a lower Pt loading than the reference, except FA-40 (same Pt loading: 37 wt.%).

Fig. 5 shows the *SA* and *MA* improvement factors of the synthesized catalysts compared to the reference catalyst. The improvement factor is defined as the ratio between the *SA* (or *MA*) of the studied catalyst and the *SA* (or *MA*, respectively) of the reference catalyst. In Fig. 5, the horizontal black line (improvement factor equal to 1) indicates the position of the reference catalyst. If the improvement factor is higher than 1, it means that the catalyst exhibits better activity than the

reference. Otherwise, if the improvement factor is lower than 1, it means that the catalyst exhibits lower activity than the reference.

The first studied synthesis was the SEA method. The size homogeneity and cleanliness of the particles yield high *SA* and high *MA*. This is shown by the *SA* and the *MA* improvement factors (Fig. 5). All the SEA catalysts display *SA* and *MA* improvement factor slightly higher than 1. Therefore, the SEA method allows producing catalysts with good performances compared to the commercial reference. However, its two major drawbacks are (i) the loss of Pt ions in the impregnation solution, as all the metal precursor can not adsorb on the CX support, and (ii) the complexity of the processing, *i.e.* the number of steps needed to reach high Pt loading. Thereupon, two other methods were developed in order to overcome these disadvantages: the CEDI method, which avoids any Pt losses, and the SB reduction, which renders the intermediate drying step useless, as the reduction occurs in liquid phase.

Concerning the performance of the CEDI and CEDI723 catalysts, the results are dependent on the reduction. The CEDI catalysts exhibit the higher *SA* because of the covering of the small Pt particles surface by chlorine. Indeed, chlorine adsorbs stronger on small Pt particles than on large Pt particles [41,42]. This implies that only the large particles, in which the Pt surface atoms are more active, could get rid of the chlorine, be detected by CO stripping, and used during the oxygen reduction. This high activity over a small surface leads to very high *SA* (improvement factor up to 2) but to very low *MA* (the lowest of all catalysts, with improvement factors below 0.75). The opposite effects occur to the CEDI723 catalysts. Their *SA* are very low as they are mainly constituted of small particles which are less active but with higher surface. Nevertheless, the high surface area values leads to high *MA*, and even to one of the best *MA* of this study (improvement factors *ca.* 1.2, in the same order than the SEA catalysts).

Concerning the catalytic activities of SB and SB723 catalysts, the *SA* values of the SB723 catalysts are low (improvement factor *ca.* 0.5) but remain similar to those of the SB catalysts (around 0.5, except for SB/8). This is due to the wide PSD (Fig. 2e) and to the high temperature reduction treatment. Indeed, the high temperature reduction treatment sinters the Pt particles and consequently increases the *SA*. However, the high temperature reduction treatment also cleans the surface of the Pt particles, especially the smallest ones, which display low *SA*. These two opposite phenomenon compensate each other, yielding almost no evolution of the *SA*. The *MA* of the SB723 catalysts are higher than those of SB catalysts reaching a maximum improvement factor of 1.1. The good *MA* is due to the high S_{CO} values, which compensate for low *SA*. However, the *MA* improvement factors are lower than those of the CEDI723 and SEA catalysts.

The previous methods allow to synthesize Pt/CX catalysts with good electrochemical activities. However, these multiple impregnation-reduction synthesis procedures need a lot of steps (impregnation, drying, reduction, *etc.*) and time in order to obtain highly loaded catalysts. This is why one-step deposition syntheses were also developed.

It was first attempted to deposit 20 wt.% of Pt by SB reduction in one single step. The physicochemical properties of SB-20 are similar to those of the SB and SB723 series. Concerning the electrochemical activities, the high *SA* of SB-20 is caused by the large particles, which are the most active towards the oxygen reduction while the small ones are probably inactive due to chlorine poisoning. However, even if the *SA* value of SB-20 is higher than that of Ref (0.121 *vs.* 0.091 A m_{Pt}^{-2}), the *MA* value of SB-20 becomes similar to that of Ref, as SB-20 displays a low S_{CO}.

The high temperature reduction was not performed on SB-20 in order to keep the synthesis method simple. Nonetheless, this treatment may decrease the activities. Indeed, SB-20 can be compared to SB/8 as they display similar physicochemical and electrochemical properties. The high temperature reduction was performed on SB/8, leading to SB723/8 catalyst. The high temperature reduction performed on SB/8 cleaned the surface of the small Pt particles, but led to sintering of the aggregates to form larger particles (see, amongst others, the evolution of S_{CO}, as well as CO stripping and XRD curves between SB/8 and SB723/8 catalysts; Table 5, Figs. 3d, e and 4d, e). This treatment decreases *SA* from 0.097 to 0.051 A m_{Pt}^{-2} (Table 5). Anyway, even if the high temperature reduction increases the S_{CO} value (from 92 to 129 m^2 g_{Pt}^{-1}), this does not compensate the decrease of *SA*, leading to low *MA* value of 6.6 A g_{Pt}^{-1} (Table 5). So, considering the similarity between SB/8 and SB-20, one can assume that the high temperature reduction would have decreased the *SA* and *MA* of SB-20 catalyst, as it was the case for SB/8 catalyst.

The catalysts synthesized by FA reduction display high *SA*, leading to an improvement factor up to 1.5 for FA-40. As they exhibit high S_{CO}, *MA* values are the highest obtained in this work. This is due to the homogeneity and the appropriate particle size. The FA catalysts can be compared with the SEA catalysts; they both exhibit a good homogeneity in particle size, *i.e.* a narrow PSD, but the FA catalysts display slightly larger particles than SEA catalysts. These larger particles are closer to the optimum particle size, which explains the better activity of the FA catalysts. Moreover, given the good catalytic performance observed and the good consistency between the physicochemical and the electrochemical results, one can assume that the formic acid reduction cleans a large part of the Pt particle surface from the poisoning chlorine. Indeed, in the FA series, SA and MA values are relatively constant (0.9–1.0 A m_{Pt}^{-2} and 10–11 A g_{Pt}^{-1}, respectively) except for FA-40, which displays (i) a higher SA value (0.138 A m_{Pt}^{-2}) and (ii) a lower MA value (8.1 A g_{Pt}^{-1}). This result is typical of a catalyst with a lower amount of very active sites. Since the dispersion of all the FA catalysts is the same, the activity difference of FA-40 could come from residual Cl still poisoning the less active Pt sites (located on edges or corners). Possibly, in the case of very high loadings, reduction with FA is not completely achieved and should be prolonged or completed with a final reduction treatment (under H_2).

The last method studied in this work was the Colloid synthesis. Col and FA catalysts display comparable S_{CO} values because (i) Col catalysts display lower Pt loading than FA catalysts and (ii) the area under the peaks of the CO stripping voltammograms of Col catalysts is lower than that of FA catalysts. However, the Col catalysts exhibit relatively low activity for the oxygen reduction (average *SA* and *MA* improvement factors equal to 0.8 and 0.9, respectively). This low activity may have three causes: (i) the Pt particle size is neither optimal nor homogeneous; (ii) some tSC may remain adsorbed on the Pt surface despite multiple washings; and (iii) the interactions between the CX support and the Pt particles may be low as the latter are synthesized in solution before contact with the CX. In any case, the Col synthesis leads to catalysts with lower catalytic activity than the best catalysts of this work or than the reference commercial catalyst.

5. Conclusion

The purpose of this work was to study various methods to synthesize electrocatalysts constituted of Pt nanoparticles deposited on carbon xerogel (Pt/CX) and to determine the impact of the synthesis process on the catalysts performance for the oxygen reduction reaction (ORR). The final aim is to simplify the process at best to allow easy scale-up while keeping optimal properties for PEMFC applications.

Starting from the strong electrostatic adsorption (SEA), the synthesis method of Pt/CX catalysts was streamlined in order to overcome the two major drawbacks of the SEA: the Pt loss and the long time needed to achieve a high Pt loading, as the impregnation-drying-reduction steps must be repeated (maximum 8 wt.% of Pt deposited after the first step). To do so, two other synthesis methods were studied: (i) the charge enhanced dry impregnation (CEDI) which avoids any Pt losses as the exact amount of Pt is used during impregnation and (ii) the reduction with sodium borohydride (SB) in liquid phase, which allows to simplify and speed up the synthesis as the drying step is avoided. However, both methods are not simple enough to scale up, as they also

need several deposition steps in order to reach high Pt loadings. Therefore, three synthesis methods, which allow to deposit a chosen amount of Pt in one single step without any Pt loss, *i.e.* one-step methods, were studied. The first one-step synthesis was based on the SEA method with reduction of a high amount of Pt in liquid phase with SB. The second synthesis was the liquid-phase reduction using formic acid (FA), a weaker reductant which allows a better control of the Pt reduction. The third method was the colloid synthesis, in which trisodium citrate was used to synthesize a Pt colloid before mixing CX to deposit the Pt particles onto the carbon support.

The best catalysts of this study were those synthesized *via* the SEA, the CEDI (both after reduction at 723 K), and the FA methods. Indeed, they result in catalysts with narrow particle size distribution close to the optimal size of 3–4 nm. The very good electrochemical properties obtained are ascribed to the size homogeneity and cleanliness of the Pt particles since: (i) large Pt particles are avoided and (ii) Cl coming from the Pt precursors is (in most cases) entirely removed. Among them, only the FA synthesis allows to synthesize highly active Pt/CX catalysts with various loading (from 10 to 40 wt.% at least) in one single deposition step. As a result, this method is better suited for scale-up. Regarding one-step processes, Pt losses are still observed when the catalysts are prepared by liquid phase reduction using formic acid; in addition, these losses seem at random, and do not seem to depend on the targeted loading. Although these losses are much smaller than in the case of other techniques (notably SEA or one-step colloid synthesis procedures), this remains an issue that has to be tackled for synthesis scale-up.

Future works will be dedicated to the study of the durability and the behaviour of the best catalysts (FA catalysts), first in liquid electrolyte with a three-electrode setup, then in PEMFCs. Another perspective is to increase the catalyst intrinsic activity by adapting the syntheses described in this work in order to synthesize Pt alloys with some transition metals (Pt-M) like Ni, Co, *etc.* The synthesis of Pt-M alloys could be considered using simultaneous or successive deposition of Pt and transition metal using techniques based on adsorption, such as the SEA method. Another investigation field could be the adaptation of one-step methods, such as FA reduction or colloid formation, in order to synthesize bimetallic nanoparticles on CX supports.

Acknowledgements

The authors thank the Walloon Region (Project HYLIFE – Grant No. 1410135) and the Fonds de Bay for funding. AZ wants to thank Dr. Ir. Pierre-Yves Olu for fruitful discussions.

Appendix A. Supplementary data

Supplementary data associated with this article can be found, in the online version, at https://doi.org/10.1016/j.apcatb.2017.11.059.

References

[1] H.A. Gasteiger, S.S. Kocha, B. Sompalli, F.T. Wagner, Activity benchmarks and requirements for Pt, Pt-alloy, and non-Pt oxygen reduction catalysts for PEMFCs, Appl. Catal. B: Environ. 56 (1-2) (2005) 9–35, http://dx.doi.org/10.1016/j.apcatb.2004.06.021 http://linkinghub.elsevier.com/retrieve/pii/S0926337304004941.

[2] H.A. Gasteiger, M.F. Mathias, Fundamental research and development challenges in polymer electrolyte fuel cell technology, in: M. Murthy (Ed.), Proceedings of the 3rd Symposium on Proton Conducting Membrane Fuel Cells, Electrochemical Society, Salt Lake City, United States of America, 2002, pp. 1–24.

[3] C. Jaffray, G.A. Hards, Precious metal supply requirements, in: W. Vielstich, A. Lamm, H.A. Gasteiger (Eds.), Handbook of Fuel Cells – Fundamentals, Technology and Applications, vol. 3, Wiley, Chichester, United Kingdom, 2003, p. 509 (Chapter 41).

[4] F. Maillard, S. Pronkin, E.R. Savinova, Influence of size on the electrocatalytic activities of supported metal nanoparticles in fuel cells related reactions, in: W. Vielstich, H.A. Gasteiger, H. Yokokawa (Eds.), Handbook of Fuel Cells, vol. 5, John Wiley & Sons, Ltd, Chichester, United Kingdom, 2009, pp. 91–111, , http://dx.doi.org/10.1002/9780470974001.f500002a https://doi.org/.%20http://dx.doi.org/%2010.1002/9780470974001.f500002a.

[5] K. Kinoshita, Particle size effects for oxygen reduction on highly dispersed platinum in acid electrolytes, J. Electrochem. Soc. 137 (3) (1990) 845–848, http://dx.doi.org/10.1149/1.2086566 http://jes.ecsdl.org/content/137/3/845?related-urls=yes&legid=jes;137/3/845.

[6] O. Antoine, Y. Bultel, R. Durand, Oxygen reduction reaction kinetics and mechanism on platinum nanoparticles inside Nafion®, J. Electroanal. Chem. 499 (1) (2001) 85–94, http://dx.doi.org/10.1016/S0022-0728(00)00492-7 http://linkinghub.elsevier.com/retrieve/pii/S0022072800004927.

[7] C. Coutanceau, S. Brimaud, C. Lamy, J.-M. Léger, L. Dubau, S. Rousseau, F. Vigier, Review of different methods for developing nanoelectrocatalysts for the oxidation of organic compounds, Electrochim. Acta 53 (23) (2008) 6865–6880, http://dx.doi.org/10.1016/j.electacta.2007.12.043 http://linkinghub.elsevier.com/retrieve/pii/S0013468607015071.

[8] F. Maillard, N. Job, M. Chatenet, Approaches to synthesize carbon-supported platinum-based electrocatalysts for proton-exchange membrane fuel cells, in: S. Suib (Ed.), New and Future Developments in Catalysis, 1st ed., Elsevier, 2013, pp. 407–428, , http://dx.doi.org/10.1016/B978-0-444-53880-2.00019-3 http://linkinghub.elsevier.com/retrieve/pii/B9780444538802000193.

[9] H. Boennemann, G. Khelashvili, Efficient fuel cell catalysts emerging from organometallic chemistry, Appl. Organomet. Chem. (2010) 257–268, http://dx.doi.org/10.1002/aoc.1613.

[10] E. Lebègue, S. Baranton, C. Coutanceau, Polyol synthesis of nanosized Pt/C electrocatalysts assisted by pulse microwave activation, J. Power Sources 196 (3) (2011) 920–927, http://dx.doi.org/10.1016/j.jpowsour.2010.08.107 http://linkinghub.elsevier.com/retrieve/pii/S0378775310015922.

[11] P. Favilla, J. Acosta, C. Schvezov, D. Sercovich, J. Collet-Lacoste, Size control of carbon-supported platinum nanoparticles made using polyol method for low temperature fuel cells, Chem. Eng. Sci. 101 (2013) 27–34, http://dx.doi.org/10.1016/j.ces.2013.05.067 http://linkinghub.elsevier.com/retrieve/pii/S0009250913004089.

[12] R. Maric, Spray-based and CVD processes for synthesis of fuel cell catalysts and thin catalyst layers, in: J. Zhang (Ed.), PEM Fuel Cell Electrocatalysts and Catalyst Layers, Springer London, London, 2008, pp. 917–963, , http://dx.doi.org/10.1007/978-1-84800-936-3_20 http://link.springer.com/.%20http://dx.doi.org/%2010.1007/978-1-84800-936-3_20.

[13] M. Vorokhta, I. Khalakhan, M. Václavu, G. Kovács, S.M. Kozlov, P. Kúš, T. Skála, N. Tsud, J. Lavková, V. Potin, I. Matolínová, K.M. Neyman, V. Matolín, Surface composition of magnetron sputtered Pt-Co thin film catalyst for proton exchange membrane fuel cells, Appl. Surf. Sci. 365 (2016) 245–251, http://dx.doi.org/10.1016/j.apsusc.2016.01.004 http://linkinghub.elsevier.com/retrieve/pii/S0169433216000180.

[14] A. Caillard, C. Charles, R. Boswell, A. Meige, P. Brault, Deposition of platinum catalyst by plasma sputtering for fuel cells: 3D simulation and experiments, Plasma Sources Sci. Technol. 17 (3) (2008) 035028, http://dx.doi.org/10.1088/0963-0252/17/3/035028 http://stacks.iop.org/0963-0252/17/i=3/a=035028?key=crossref.5fc235b8bbb8c87b50176267936a4a2e.

[15] E. Antolini, Carbon supports for low-temperature fuel cell catalysts, Appl. Catal. B: Environ. 88 (1-2) (2009) 1–24, http://dx.doi.org/10.1016/j.apcatb.2008.09.030 http://linkinghub.elsevier.com/retrieve/pii/S0926337308003809.

[16] M.S. Saha, V. Neburchilov, D. Ghosh, J. Zhang, Nanomaterials-supported Pt catalysts for proton exchange membrane fuel cells, Wiley Interdiscip. Rev.: Energy Environ. 2 (1) (2013) 31–51, http://dx.doi.org/10.1002/wene.47 http://doi.wiley.com/10.1002/wene.47.

[17] J. Marie, S. Berthon-Fabry, P. Achard, M. Chatenet, A. Pradourat, E. Chainet, Highly dispersed platinum on carbon aerogels as supported catalysts for PEM fuel cell-electrodes: comparison of two different synthesis paths, J. Non-Cryst. Solids 350 (2004) 88–96, http://dx.doi.org/10.1016/j.jnoncrysol.2004.06.038 http://linkinghub.elsevier.com/retrieve/pii/S0022309304008312.

[18] N. Job, J. Marie, S.D. Lambert, S. Berthon-Fabry, P. Achard, Carbon xerogels as catalyst supports for PEM fuel cell cathode, Energy Convers. Manag. 49 (9) (2008) 2461–2470, http://dx.doi.org/10.1016/j.enconman.2008.03.025 http://www.sciencedirect.com/science/article/pii/S0196890408001246.

[19] B. Liu, S. Creager, Carbon xerogels as Pt catalyst supports for polymer electrolyte membrane fuel-cell applications, J. Power Sources 195 (7) (2010) 1812–1820, http://dx.doi.org/10.1016/j.jpowsour.2009.10.033 http://linkinghub.elsevier.com/retrieve/pii/S0378775309018370.

[20] C. Alegre, L. Calvillo, R. Moliner, J. González-Expósito, O. Guillén-Villafuerte, M.M. Huerta, E. Pastor, M. Lázaro, Pt and PtRu electrocatalysts supported on carbon xerogels for direct methanol fuel cells, J. Power Sources 196 (9) (2011) 4226–4235, http://dx.doi.org/10.1016/j.jpowsour.2010.10.049 http://linkinghub.elsevier.com/retrieve/pii/S0378775310018483.

[21] J. Calderón, N. Mahata, M. Pereira, J. Figueiredo, V. Fernandes, C. Rangel, L. Calvillo, M. Lázaro, E. Pastor, Pt-Ru catalysts supported on carbon xerogels for PEM fuel cells, Int. J. Hydrogen Energy 37 (8) (2012) 7200–7211, http://dx.doi.org/10.1016/j.ijhydene.2011.12.029 http://linkinghub.elsevier.com/retrieve/pii/S0360319911026814.

[22] A. Zubiaur, M. Chatenet, F. Maillard, S.D. Lambert, J.-P. Pirard, N. Job, Using the multiple SEA method to synthesize Pt/carbon xerogel electrocatalysts for PEMFC applications, Fuel Cells 14 (3) (2014) 343–349, http://dx.doi.org/10.1002/fuce.201300208 http://doi.wiley.com/10.1002/fuce.201300208.

[23] C. Alegre, D. Sebastián, M.E. Gálvez, R. Moliner, M.J. Lázaro, Sulfurized carbon xerogels as Pt support with enhanced activity for fuel cell applications, Appl. Catal. B: Environ. 192 (2016) 260–267, http://dx.doi.org/10.1016/j.apcatb.2016.03.070 http://linkinghub.elsevier.com/retrieve/pii/S0926337316302521.

[24] C. Alegre, D. Sebastián, M. Gálvez, E. Baquedano, R. Moliner, A. Aricò, V. Baglio, M. Lázaro, N-doped carbon xerogels as Pt support for the electro-reduction of

oxygen, Materials 10 (9) (2017) 1092, http://dx.doi.org/10.3390/ma10091092 http://www.mdpi.com/1996-1944/10/9/1092.
[25] J. Regalbuto, A. Navada, S. Shadid, M. Bricker, Q. Chen, An experimental verification of the physical nature of Pt adsorption onto alumina, J. Catal. 184 (2) (1999) 335–348, http://dx.doi.org/10.1006/jcat.1999.2471 http://www.sciencedirect.com/science/article/pii/S0021951799924715.
[26] J.R. Regalbuto, Catalyst Preparation: Science and Engineering, CRC Press/Taylor & Francis Group, Boca Raton, USA, 2006.
[27] N. Job, S.D. Lambert, M. Chatenet, C.J. Gommes, F. Maillard, S. Berthon-Fabry, J.R. Regalbuto, J.-P. Pirard, Preparation of highly loaded Pt/carbon xerogel catalysts for Proton Exchange Membrane fuel cells by the Strong Electrostatic Adsorption method, Catal. Today 150 (1–2) (2010) 119–127, http://dx.doi.org/10.1016/j.cattod.2009.06.022 http://linkinghub.elsevier.com/retrieve/pii/S092058610900354X.
[28] C. Cao, G. Yang, L. Dubau, F. Maillard, S.D. Lambert, J.-P. Pirard, N. Job, Highly dispersed Pt/C catalysts prepared by the Charge Enhanced Dry Impregnation method, Appl. Catal. B: Environ. 150 (2014) 101–106, http://dx.doi.org/10.1016/j.apcatb.2013.12.004 http://www.sciencedirect.com/science/article/pii/S0926337313007492.
[29] C. Alegre, M. Gálvez, R. Moliner, V. Baglio, A. Aricò, M. Lázaro, Towards an optimal synthesis route for the preparation of highly mesoporous carbon xerogel-supported Pt catalysts for the oxygen reduction reaction, Appl. Catal. B: Environ. 147 (2014) 947–957, http://dx.doi.org/10.1016/j.apcatb.2013.10.031 http://www.sciencedirect.com/science/article/pii/S0926337313006565.
[30] N. Job, F. Maillard, J. Marie, S. Berthon-Fabry, J.P. Pirard, M. Chatenet, Electrochemical characterization of Pt/carbon xerogel and Pt/carbon aerogel catalysts: first insights into the influence of the carbon texture on the Pt nanoparticle morphology and catalytic activity, J. Mater. Sci. 44 (24) (2009) 6591–6600, http://dx.doi.org/10.1007/s10853-009-3581-x.
[31] A.M. Pasqualeti, P.-Y. Olu, M. Chatenet, F.H.B. Lima, Borohydride electrooxidation on carbon-supported noble metal nanoparticles: insights into hydrogen and hydroxyborane formation, ACS Catal. 5 (5) (2015) 2778–2787, http://dx.doi.org/10.1021/acscatal.5b00107 http://pubs.acs.org/doi/abs/10.1021/acscatal.5b00107.
[32] M.-L.C. Piedboeuf, A.F. Léonard, K. Traina, N. Job, Influence of the textural parameters of resorcinol-formaldehyde dry polymers and carbon xerogels on particle sizes upon mechanical milling, Colloids Surf. A: Physicochem. Eng. Asp. 471 (2015) 124–132, http://dx.doi.org/10.1016/j.colsurfa.2015.02.014 http://www.sciencedirect.com/science/article/pii/S0927775715001375.
[33] N. Job, M. Chatenet, S. Berthon-Fabry, S. Hermans, F. Maillard, Efficient Pt/carbon electrocatalysts for proton exchange membrane fuel cells: avoid chloride-based Pt salts!, J. Power Sources 240 (2013) 294–305, http://dx.doi.org/10.1016/j.jpowsour.2013.03.188 http://www.sciencedirect.com/science/article/pii/S0378775313006010.
[34] G. Bergeret, P. Gallezot, Particle size and dispersion measurement, in: G. Ertl, H. Knözinger, J. Weitkamp (Eds.), Handbook of Heterogeneous Catalysis, Wiley-VCH, Weinheim, Germany, 1997, p. 439.
[35] E. Guilminot, A. Corcella, M. Chatenet, F. Maillard, Comparing the thin-film rotating disk electrode and the ultramicroelectrode with cavity techniques to study carbon-supported platinum for proton exchange membrane fuel cell applications, J. Electroanal. Chem. 599 (1) (2007) 111–120, http://dx.doi.org/10.1016/j.jelechem.2006.09.022 http://www.sciencedirect.com/science/article/pii/S0022072806005559.
[36] F. Maillard, M. Eikerling, O.V. Cherstiouk, S. Schreier, E. Savinova, U. Stimming, Size effects on reactivity of Pt nanoparticles in CO monolayer oxidation: the role of surface mobility, Faraday Discuss. 125 (2004) 357, http://dx.doi.org/10.1039/b303911k http://pubs.rsc.org/en/content/articlehtml/2004/fd/b303911k.
[37] F. Maillard, S. Schreier, M. Hanzlik, E.R. Savinova, S. Weinkauf, U. Stimming, Influence of particle agglomeration on the catalytic activity of carbon-supported Pt nanoparticles in CO monolayer oxidation, Phys. Chem. Chem. Phys. 7 (2) (2005) 385–393, http://dx.doi.org/10.1039/B411377B http://pubs.rsc.org/en/content/articlehtml/2005/cp/b411377b.
[38] F. Maillard, E.R. Savinova, U. Stimming, CO monolayer oxidation on Pt nanoparticles: further insights into the particle size effects, J. Electroanal. Chem. 599 (2) (2007) 221–232, http://dx.doi.org/10.1016/j.jelechem.2006.02.024 http://www.sciencedirect.com/science/article/pii/S002207280600115X.
[39] S. Trasatti, O. Petrii, Real surface area measurements in electrochemistry, J. Electroanal. Chem. 327 (1–2) (1992) 353–376, http://dx.doi.org/10.1016/0022-0728(92)80162-W http://www.sciencedirect.com/science/article/pii/002207289280162W.
[40] A.J. Bard, L.R. Faulkner, Electrochemical Methods: Fundamentals and Applications, 2nd ed., John Wiley & Sons, Inc., Weinheim, Germany, 2001http://tocs.ulb.tu-darmstadt.de/95069577.pdf.
[41] Z.C. Zhang, B.C. Beard, Genesis of durable catalyst for selective hydrodechlorination CCl_4 to $CHCl_3$ [A4281], Appl. Catal. 174 (1–2) (1998) 33, http://dx.doi.org/10.1016/S0926-860X(98)00150-1 http://linkinghub.elsevier.com/retrieve/pii/S0926860X98001501.
[42] B. Coq, G. Ferrat, F. Figueras, Conversion of chlorobenzene over palladium and rhodium catalysts of widely varying dispersion, J. Catal. 101 (2) (1986) 434–445, http://dx.doi.org/10.1016/0021-9517(86)90271-X http://linkinghub.elsevier.com/retrieve/pii/002195178690271X.